EUROPEAN ORGANIZATION FOR NUCLEAR RESEARCH
European Laboratory for Particle Physics

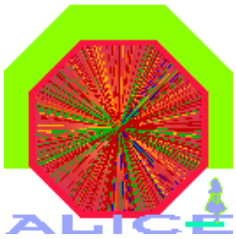

Internal Note/PHOS
ALICE reference number
ALICE-INT-2005-014 version 3.0
Institute reference number
[-]
Date of last change
2005-06-03

Prompt photon and photon-tagged jets identification with ALICE

Authors:

G. Conesa[1], H. Delagrange[2], J. Diaz[1], Y. V. Kharlov[3], Y. Schutz[2,4]

[1]IFIC (Cnetro Mixto Universidad de Valencia-CSIC), Valencia, Spain
[2]SUBATECH, UMR6457 (Ecole des Mines-IN2P3/CNRS-Université de Nantes
[3]Institute for High-Energy Physics, Protvino, Russia
[4]CERN, Genève, Switzerland

Abstract:

The ALICE experiment at LHC will detect and identify prompt photons and light neutral-mesons with the PHOS detector and, subject to approval, with the EMCal detector. Charged particles will be detected and identified by the central tracking system. The possibility to tag jets with photons is examined. Methods to identify prompt photons and prompt photon-jet events, and distinguish them against the background of decay photons, are discussed.

Prompt photon and photon-tagged jets identification with ALICE

27th September 2005

G. Conesa[1], H. Delagrange[2], J. Díaz[1], Y.V. Kharlov[3], Y. Schutz[2,4]

Abstract

The ALICE experiment at LHC will detect and identify prompt photons and light neutral-mesons with the PHOS detector and, subject to approval, with the EMCal detector. Charged particles will be detected and identified by the central tracking system. The possibility to tag jets with photons is examined. Methods to identify prompt photons and prompt photon-jet events, and distinguish them against the background of decay photons, are discussed.

Contents

[1]IFIC (Centro Mixto Universidad de Valencia-CSIC), Valencia, Spain
[2]SUBATECH, UMR6457 (Ecole des Mines-IN2P3/CNRS-Université de Nantes), BP20722, 44307 Nantes CEDEX 3, France
[3]Institute for High-Energy Physics, Protvino, Russia
[4]CERN, Genève, Switzerland

Introduction

The experimental study of hadron jets at LHC will play a central role in understanding the properties of the quark gluon plasma (QGP) formed in ultra-relativistic nucleus-nucleus collisions [1]. Hadron jets are generated by hadronization of a final-state parton shower originated by high transverse momentum (p_T) partons scattered in primary partonic collisions involving a hard perturbative scale ($Q \gg \Lambda_{QCD},\ T$, where T is the initial temperature of the medium formed in the heavy-ion collision). As early as in 1982, J.D. Bjorken suggested [2] that partons propagating through a nuclear medium will suffer an energy loss whose magnitude is strongly dependent on the color charge density of the traversed medium. The medium induced modification experienced by the parton will be reflected in the properties of the final state jet of hadrons. In particular, the energy loss of the parton will show up in a modification of the energy spectrum of the jet hadrons, the so called jet quenching effect. Such an effect has indeed been observed [3–6] in central Au-Au collisions at $\sqrt{s_{NN}} = 130$ and 200 GeV by various RHIC experiments in measurements of high p_T charged and neutral hadrons ($p_T \sim 2 - 15$ GeV/c), which are at present the only observable, together with hadron jet back-to-back correlations [7], within reach for the study of partons interacting with deconfined matter. As a matter of fact, yields of inclusive charged hadrons and π^o mesons are suppressed by as much as a factor of 4-5, independent of the p_T value, compared to pp and peripheral Au-Au yields, properly scaled.

The ALICE experiment will extend such studies at higher $\sqrt{s}$. Because of the higher cross sections for hard processes, jets will be abundantly produced at LHC (10^5 jets with $p_T > 100$ GeV/c per year) enabling inclusive and exclusive jet measurements. In particular, jet topology (jet shape, jet *heating*, fragmentation function...) will be measured to study the redistribution of the energy of the jet traversing the medium [8]. Such studies require the identification of jets and the measurement, as accurately as possible, of the parton or jet energy, ideally before and after quenching. A very attractive method to perform these studies is to tag jets with prompt photons emitted in the opposite direction to the jet direction. The dominant processes for such events are $g + q \rightarrow \gamma + q$ (Compton) and $q + \bar{q} \rightarrow \gamma + g$ (annihilation), although recent studies [9] show that below 50 GeV/c bremsstrahlung contribute significantly to the photon spectrum. Photons emerge almost unaltered from the dense medium and provide a measurement of the original energy of the parton emitted in the op-

Detector	$\|\eta\|$	ϕ_{min}	ϕ_{max}
PHOS	0.12	220^o	320^o
EMCal	0.7	60^o	180^o
TPC	0.7	0^o	360^o

Table 1: TPC, PHOS and EMCal acceptances. The physical TPC η acceptance is larger ($|\eta| < 0.9$), but we select this lower value to ensure a good track matching.

posite direction. On one hand, this coincidence technique will help to localize the jet and on the other hand allows to build the parton fragmentation function without the need to reconstruct the jet energy from the detected hadrons. Medium effects will then be identified through modifications of the fragmentation function, i.e. the redistribution of the jet energy rather than by its reduction.

In ALICE, photons will be detected by PHOS [10] which enables to measure with high precision their 4-momentum, however, only with a limited acceptance. The identification power of prompt photons at low p_T is limited by the background created by decay photons (mainly, $\pi^0 \rightarrow \gamma + \gamma$). At higher p_T, where the γ/π^0 ratio increases, the merging of the decay photons into a single shower mimicking a single photon limits the identification of prompt photons. The identification of photon-jet events in ALICE is optimal for photons with energy larger than 20 GeV. Below this value, decay and prompt photons cannot be efficiently distinguished on an event by event basis. In the present note, we discuss the feasibility of identifying prompt photons and photon-jet events in *pp* and heavy-ion collisions and the possibility to gain valuable information on medium modification of hard parton properties. First, we present methods to identify photons (prompt or decay) and to discriminate them from charged hadrons. Decay photons are further identified by shower topology analysis and isolation criteria. Next, we discuss an algorithm to identify photon-jet events and to reconstruct the hadron jet features. In the reconstruction procedure, two experimental configurations are considered: i) only charged particles are detected in the ALICE central tracking system and ii) in addition neutral particles are detected by an electromagnetic calorimeter[5].

A forthcoming paper will discuss the observables to identify and analyze medium modification.

1 Event simulation and detection main reconstruction features

Prompt photons are detected by PHOS whereas charged particles streaming from jets are detected by the ALICE central tracking system, TPC, and neutral jet particles in the electromagnetic calorimeter EMCal (if available). The acceptances of all the detectors involved are reported in Tab. 1 and their location pictured in Fig. 1.

For event generation, we consider prompt photon production in the leading order

[5]Electromagnetic calorimeter presently under discussion in the US [11].

of the Standard Model. The dominant parton-level subprocesses contributing are

$$\begin{array}{rcl} g+q & \rightarrow & \gamma+q, \\ q+\bar{q} & \rightarrow & \gamma+g. \end{array} \tag{1}$$

These processes were simulated by the event generator PYTHIA 6.203 [12,13] in pp collisions at $\sqrt{s} = 5.5$ TeV. The default parton distribution function, GRV 94L [14], was used. Since the production cross sections drop very quickly with p_T, events were sampled in $\langle p_T \rangle$[6] bins (about 10,000 events per bin) : $[20, 40]$, $[40, 60]$, $[60, 80]$, and $[80, 100]$ GeV/c. To obtain the continuous differential cross sections over the whole p_T-range, these four samples were combined with weights corresponding to their cross sections as calculated by PYTHIA. To enrich the sample with events detected in PHOS, we restrict in the event generation, the prompt photon pseudorapidity in the event center-of-mass system to $|\eta_\gamma| < 0.2$, and considering the following angular aperture $200^\circ < \phi_\gamma < 340^\circ$. The solid angle containing the generated particles is taken slightly wider than the detector acceptance to avoid possible boundary effects. From now on, we will refer to such kind of events as γ-jet. We performed also a few γ-jet simulations with mono-energetic photons ($\Delta E = 0.1$ GeV) of 5, 10, 20, 40, 60 and 80 GeV, to test at higher statistics the jet reconstruction capability of our algorithm with well defined jet energies (see Sec. 4.3).

As they are significant sources of background, hard QCD $2 \rightarrow 2$ subprocesses in the leading pQCD order were also considered,

$$\begin{array}{rcl} q+q & \rightarrow & g+g, \\ q+q' & \rightarrow & q+q', \\ q+\bar{q} & \rightarrow & q+\bar{q}, \\ q+g & \rightarrow & q+g, \\ g+g & \rightarrow & g+g, \\ g+g & \rightarrow & q+q'. \end{array} \tag{2}$$

These subprocesses contribute to the background as hard fragmentation π^0-mesons. Their decay photons are detected in PHOS as a single electromagnetic shower and, hence, mimic prompt photons. There is also the bremsstrahlung process to be considered as background contribution. To simulate a continuous p_T-spectrum of π^0-mesons from 20 to 100 GeV/c, we generated hard QCD processes in eight bins of 10 GeV/c in the $\langle p_T \rangle$ range from 30 to 100 GeV/c and in four more bins of 50 GeV/c in the $\langle p_T \rangle$ range from 100 to 300 GeV/c (about 150,000 events per bin). The full p_T spectrum is the combination of these event samples weighted by their corresponding cross sections. The generation of hard QCD processes was restricted in process center-of-mass system to $|y_{parton}| < 0.2$ and in the event center-of-mass system to $|\eta_{jet}| < 0.15$, without any azimuth limitation. In the jet-jet case, we needed to apply a more severe restriction in rapidity than in the γ-jet case because of the small PHOS acceptance, the background statistics is low with wider rapidity ranges. From now on we will refer to such kind of events as jet-jet.

To simulate events corresponding to Pb-Pb collisions we have assumed that a Pb-Pb collision is equivalent to a pp collision plus a heavy-ion underlying event. Thus,

[6]Here $\langle p_T \rangle$ refers to the transverse momentum of the hard $2 \rightarrow 2$ subprocesses in their center-of-mass system.

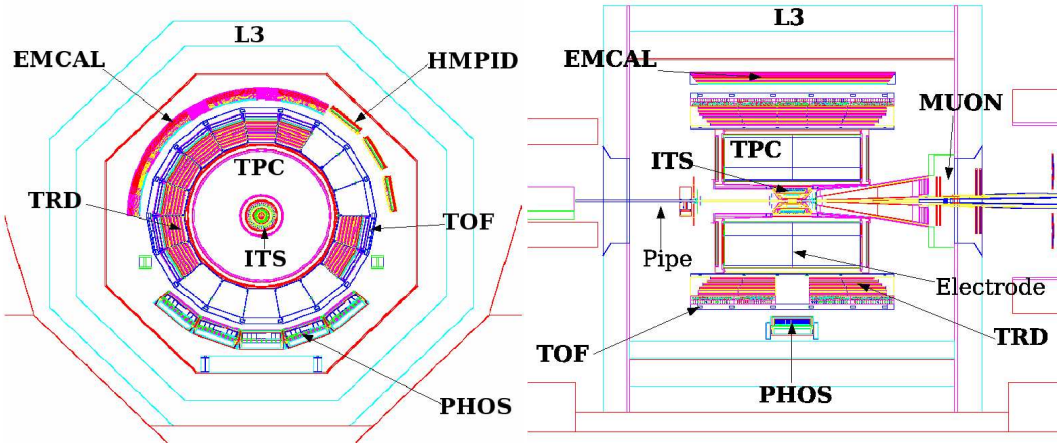

Figure 1: Layout of various ALICE detectors.

Collision	$\mathcal{L}$ (cm^{-2} s^{-1})	Time (s)	Centrality (%)	f_C	$\langle T_{AA} \rangle_C$ (mb^{-1})
pp	10^{30}	10^7			
Pb-Pb	$0.5\,10^{27}$	10^6			
Pb-Pb			5	0.05	26.0
Pb-Pb			10	0.1	23.2
Pb-Pb			Minimum bias	1	5.58

Table 2: Beam luminosity and running time for the ALICE experiment during a standard year of running at LHC. Values of the nuclear overlap functions are taken from Appendix I of [16].

pp collisions generated by PYTHIA, were merged with heavy-ion events produced by the HIJING 1.36 [15] event generator for Pb-Pb collisions at $\sqrt{s_{NN}} = 5.5A$ TeV and impact parameters $b < 2$ fm.

The aim of our investigation is to develop an algorithm capable of identifying prompt photons and γ-jet events and of minimizing misidentified jet-jet events (see Sec. 4.4). There are real discrepancies between event generators, PYTHIA (we used), HERWIG and NLO calculations. In the present state of knowledge, there are no definitive arguments in favor of one of these generators. In such circumstances we assume that PYTHIA can help us to demonstrate the validity of our approach.

1.1 Expected experimental rates

The p_T distributions obtained from simulations are normalized to the number of events expected in a standard year of running at LHC (see Tab. 2). As we have simulated different p_T bins, each one with a given number of events, we proceed in the following way:

- The raw distributions, N_i, are normalized to the number of simulated events, N_{Evt}, in each p_T bin and then to the cross sections assigned by PYTHIA

(Appendix A). Finally, the different distributions are combined to obtain the differential cross section in p_T.

- The differential cross section is multiplied by the integrated luminosity expected in one running period: luminosity $\mathcal{L}$ and running time, are listed in Tab. 2. Here we follow a quite standard procedure described in details in [17] and [16], the "binary scaling". For Pb-Pb collisions, the pp PYTHIA events are scaled by the average number of NN collisions by multiplying the corresponding differential pp cross section by the product of the nuclear overlap function $\langle T_{AA}\rangle_C$ for the appropriate centrality class C, the centrality factor f_C and the geometrical cross section $\sigma_{AA}^{geo} = 7745$ mb as postulated in Eq. (133) of [16], i.e.

$$\left(\frac{d^2\sigma_{AA}^{PYTHIA}}{dp_T dy}\right)_C = \langle T_{AA}\rangle_C \cdot \sigma_{AA}^{geo} \cdot f_C \cdot \frac{d^2\sigma_{pp}^{PYTHIA}}{dp_T dy} \tag{3}$$

  The appropriate parameter values needed are listed in Tab. 2. We consider minimum bias collisions.

This procedure leads to the expected spectra (Fig. 2) of prompt photons (γ-jet) and γ-like (jet-jet) in pp and Pb-Pb collisions at $5.5A$ TeV detected in the PHOS acceptance during a standard year of running at LHC. We denote photon-like any photon which is not a prompt photon, including bremsstrahlung and decay photons from jet-jet events, or originating from any other source. The decay photons from jet-jet events are detected in PHOS, as either single or overlapped[7]. Because of the PHOS geometry the overlapped clusters are predominant at π^0 energies beyond 40 GeV (see Fig. 4). All these photons constitute the background in the prompt photon identification and contribute (Fig. 3) predominantly to the inclusive photon spectrum.

2 Response of the detectors

In this section, we describe the response functions applied for the detectors involved in our analysis, PHOS, EMCal and the central tracking system, TPC.

The goal of the present study is to assess the performance of our identification algorithms. For this purpose a fast simulation is well suited, complete event simulation with transport and reconstruction would imply a significantly longer computing time (more elaborated simulations will be performed during the ALICE physics data challenge). In fact, in a fast simulation framework, we did rely on the properties of the final state particles generated by PYTHIA and on the knowledge of the response functions of the various detectors involved.

[7] An energetic π^o decays into two photons whose opening angle is too small to be distinguished in PHOS and generates a single cluster. We call also this kind of event one-cluster π^0.

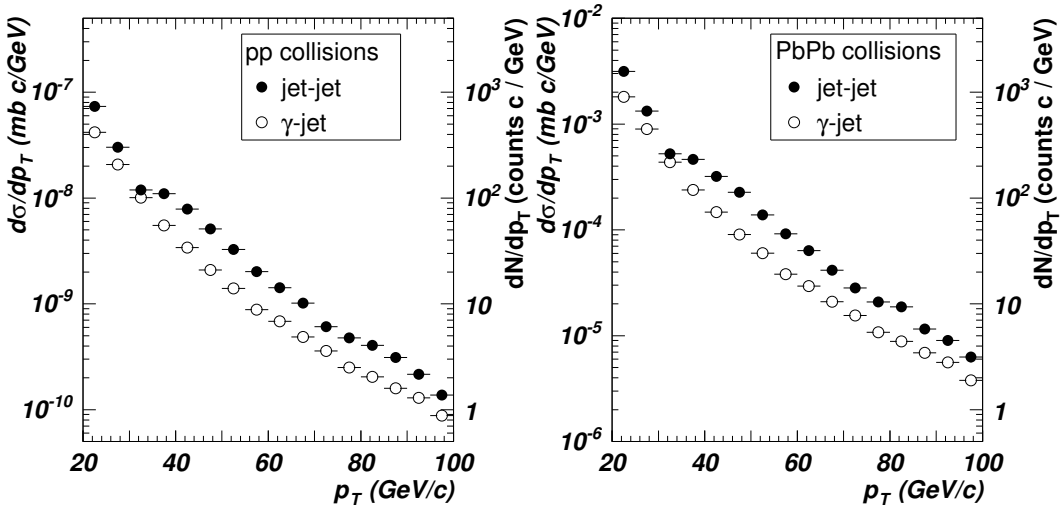

Figure 2: Spectra of prompt photons (γ-jet events, $\circ$) and γ-like (single and overlapped photons from jet-jet events, $\bullet$) detected in PHOS, for pp (left) and minimum bias Pb-Pb (right) collisions at $\sqrt{s_{NN}} = 5.5A$ TeV. Differential cross sections correspond to the left y-axis of each plot and the expected number of particles to the right y-axis. Both quantities are determined for a standard year of running at LHC.

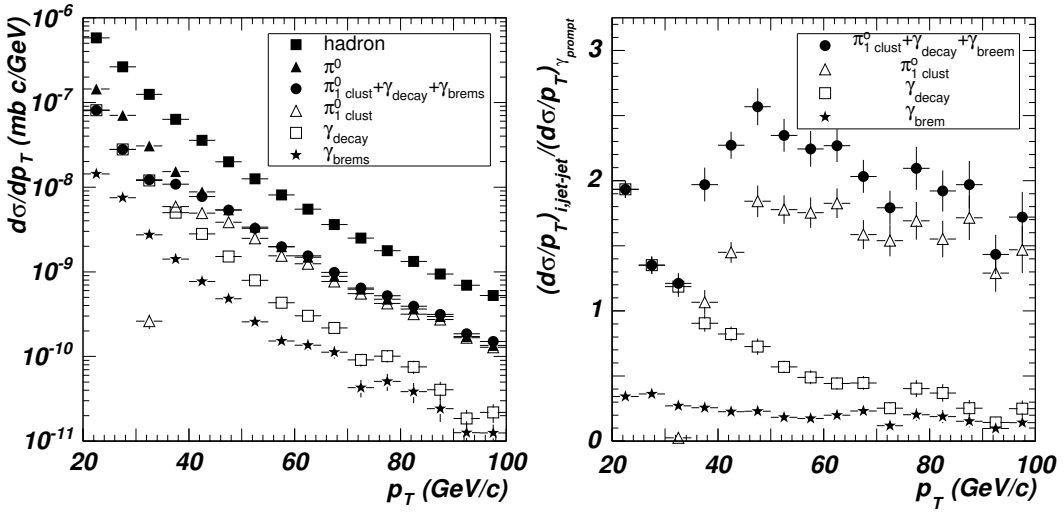

Figure 3: Left frame: Spectra of different particles, detected in PHOS, streaming from a jet-jet event in pp collisions at $\sqrt{s} = 5.5$ TeV : ($\blacktriangle$) total hard π^0's; ($\triangle$) hard π^0's that generate a single cluster in PHOS (overlapped photons from decay, it is important above 30 GeV/c); ($\square$) photons from decay (not overlapped); ($\bullet$) π^0's that generate a single cluster plus photons from decay plus photons from bremsstrahlung; ($\blacksquare$) total hadron spectrum; ($\bigstar$) photons from bremsstrahlung. Right frame: Ratio of the generated photon-like particles in jet-jet events to prompt photon in γ-jet events: π^0's that generate one cluster ($\triangle$) or two clusters ($\square$), photons from bremsstrahlung ($\bigstar$), and the sum of all of these contributions ($\bullet$).

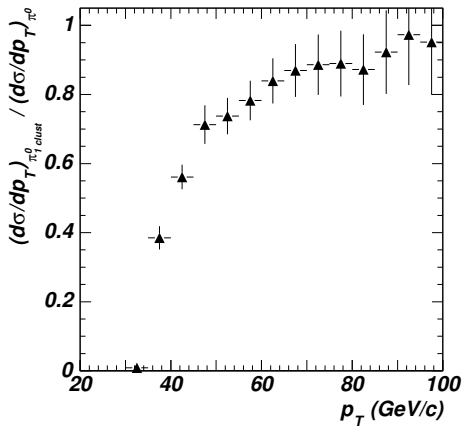

Figure 4: Ratio of the one-cluster π^0 detected in PHOS to the total generated π^0 spectrum.

2.1 Photon detectors, PHOS and EMCal

PHOS and EMCal will be the detectors dedicated to the photon detection in the ALICE experiment. As a first approximation in this investigation, the EMCal response was chosen identical to the PHOS response.

The energy and impact position for PYTHIA generated particles that fall into these detectors are smeared according to a Gaussian distribution. The width of these smearing distributions corresponds to the experimental energy and position resolutions:

$$\frac{\Delta E}{E} = \frac{0.013}{E} \oplus \frac{0.036}{\sqrt{E}} \oplus 0.0112 \tag{4}$$

$$\sigma_x = \frac{0.229}{\sqrt{E}} \oplus 0.096 \tag{5}$$

where energies are given in GeV and positions in cm. The energy resolution (Fig. 5) has been measured during electron beam tests performed with a PHOS prototype at CERN in Summer 2002. The position resolutions at different incidence angles were simulated within the frame of **AliRoot** [18] and Eq. (5) was fitted to the results (for more details see [10]). The PHOS energy threshold is 0.5 GeV and only particles depositing energy greater than this value are taken into account.

2.2 Charged particle detector

For charged particles, the fast reconstruction provides a parameterized response of ITS [19] and TPC [20] to long-lived charged particles. Within this fast reconstruction, charged particles are detected with an angular resolution of $\Delta\alpha \approx 1.1^\circ$ and a constant momentum resolution $\Delta p/p = 2\,\%$. These resolutions are the main parameters of the Gaussian smearing applied to the generated 3-momentum. After smearing the particle energy is recalculated in order to conserve the particle mass. A detection and identification probability of 80 % is considered within the pseudo-rapidity range $|\eta| < 0.7$ and at transverse momenta $p_T > 150$ MeV/c. It is null outside of these limits. All these values were extracted from [21].

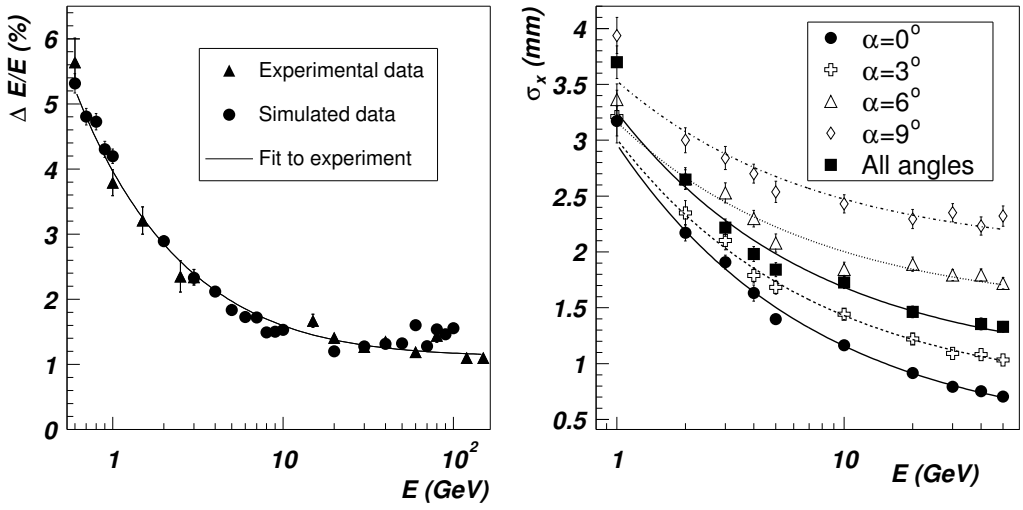

Figure 5: PHOS resolution main features. Left frame: energy resolution obtained from beam tests of a PHOS prototype, in 2002 and detector simulation. Right frame: position resolutions for different incidence angles, obtained from simulation.

3 Prompt photon identification with PHOS

In this section, the prompt photon identification is discussed together with the efficiency for rejecting the contamination due to hard π^0's. The identified prompt photon spectrum, which will be measured in one running period, will be presented.

Two procedures to select prompt photons are applied: the shower shape analysis, SSA, and the isolation cut method, ICM. The former identifies photons according to the shape of the shower which develops in the detector, and the latter tags and identifies a photon as a prompt one if it appears isolated, without charged particles found in its vicinity.

For the sake of this study, we have used the same simulated PYTHIA (pp) and PYTHIA+HIJING (Pb-Pb) events described in Sec. 1, but have however performed a fully-fledged Monte Carlo simulation for the transport of particles in PHOS. We also used the information of the charged particles collected in the acceptance of the ALICE central tracking system (only in ICM), but applying the fast reconstruction described in Sec. 2.2.

3.1 Shower shape analysis, SSA

Particles are identified in PHOS from the correlation of 3 measured parameters:

- **Charged Particle Veto (CPV)**: Charged particle identification.
- **Time Of Flight (TOF) measurement**: Identification of massive, low p_T particles .
- **Electromagnetic Calorimetry**: Photon and hadron identification through shower shape analysis.

Particles of different nature (photons, overlapped photons and hadrons) generate different shower shapes inside the calorimeter. To identify photons we use two different methods depending on the shower shape:

1. **Principal Components Analysis (PCA)**: This method combines various shower parameters in a set of two weakly correlated parameters. By appropriate cuts in the two-dimensional space of these two parameters, three classes of photons are defined depending on the purity of the identification (percentage of photons identified as photons): *low* (90-95 % efficiency), *medium* (85-90 % efficiency) and *high* (40-50 % efficiency) *purity* for single photon events.

2. **Lateral Dispersion Analysis**: The selection criterion based on the lateral dispersion of the shower has been tuned to provide an optimal rejection of overlapped-photons due to π^0's. This method is only applicable for energies larger than 30 GeV and defines a new class of photons labeled *hard dispersion photons*.

We will refer to these kinds of identification in PHOS as PID, particle identification. The TOF and CPV selections also have three different purities defined, matching those defined with the PCA. When we use the lateral dispersion analysis, the selections from the CPV and TOF are not taken into account. This analysis is explained in detail in [10].

The identified photon spectra (applying PID with medium purity level) from γ-jet and jet-jet events detected in PHOS during one running period are displayed in Fig. 6. The identification probabilities, calculated as the ratio of identified spectra (Fig. 6) to simulated spectra (Fig. 2), is for medium purity photons about 90 % in *pp* collisions and about 75 % in Pb-Pb collisions (Fig. 7). For the one-cluster π^0 for medium purity identification (Fig. 8-upper), it rises from 0 to 40 % and for hadron (Fig. 9-upper) it rises from 5 to 10 %. For medium purity identification the π^0 background (from jet-jet events) remains still too high, as can be seen in the ratio photon to π^0 of Fig. 8-lower. For higher purity and hard dispersion the rejection is better, but there is a drastic reduction of the photon identification efficiency. Additional identification procedures are therefore required.

3.2 Isolation cut method

Prompt photons are produced in parton collisions [see Eq. (1)], in which the final state photon and parton are emitted back-to-back. The photon should thus appear isolated with no hadron flying in the same direction[8]. However the underlying event generated by the heavy-ion collision, will perturb this ideal topology. To overcome this difficulty, we have developed two isolation cut methods. Both methods search around high-p_T photon candidates ($p_T > 20$ GeV/c), identified by the SSA-PID (see Sec. 3.1) for hadrons inside a cone centered along the photon direction (η_0, ϕ_0):

[8]This is not true for next to leading order processes like bremsstrahlung. However, PYTHIA predicts that such processes are suppressed compared to the ones under study (see Fig. 3). This statement might have to be revised considering recent studies [9], which suggest that at high p_T the bremsstrahlung could be a dominant process.

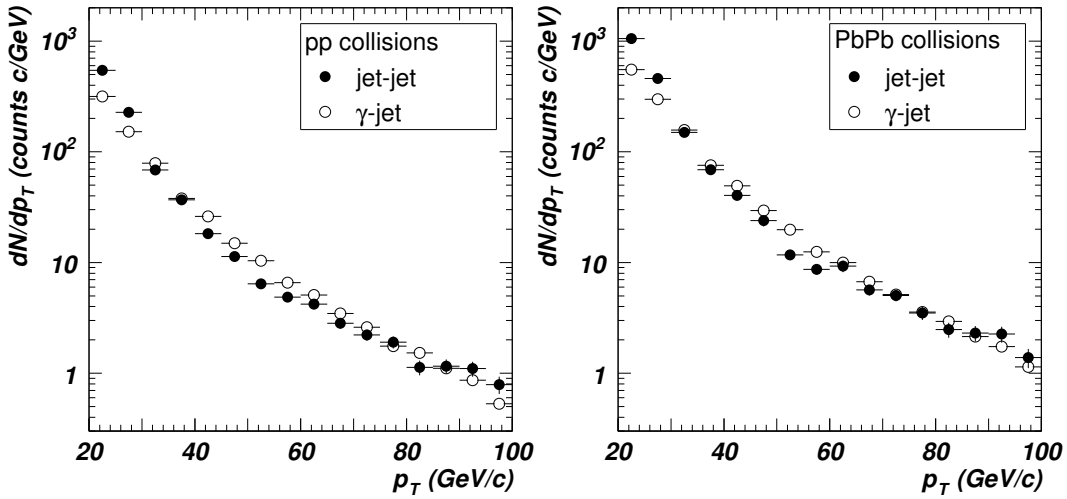

Figure 6: Identified medium purity photon spectra in jet-jet (•) and γ-jet events (◦) with shower shape analysis in pp (left) and Pb-Pb (right) collisions at $5.5A$ TeV obtained with the expected luminosity in a standard year of running at LHC.

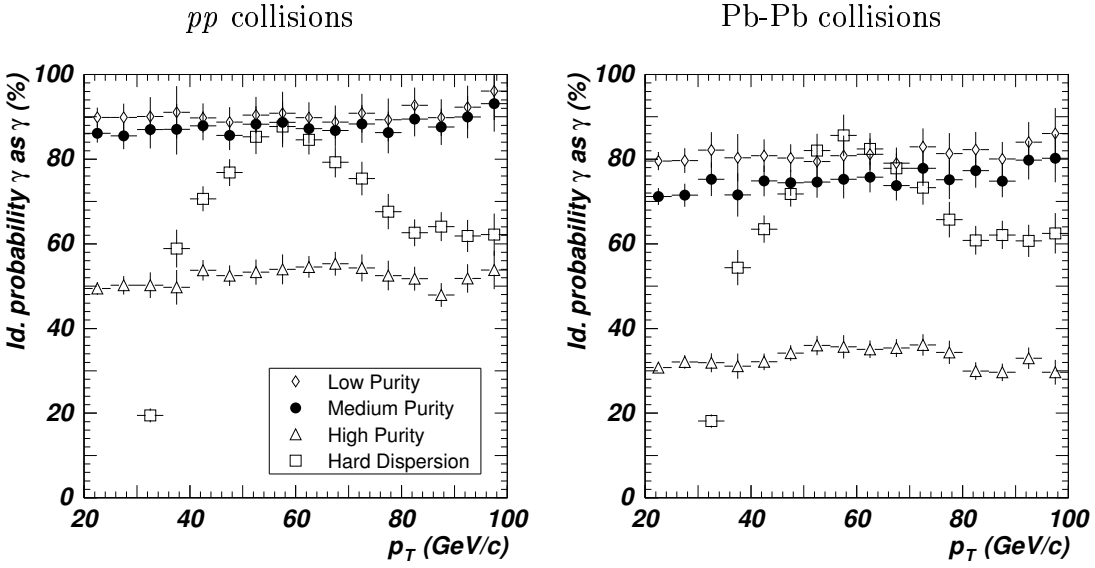

Figure 7: Probability to identify prompt photons from γ-jet events (left) detected in PHOS as photons, for pp (left) and Pb-Pb (right) collisions with shower shape analysis. Different identification purities defined for PHOS have been applied. The experimental conditions correspond to collisions at $\sqrt{s} = 5.5A$ TeV.

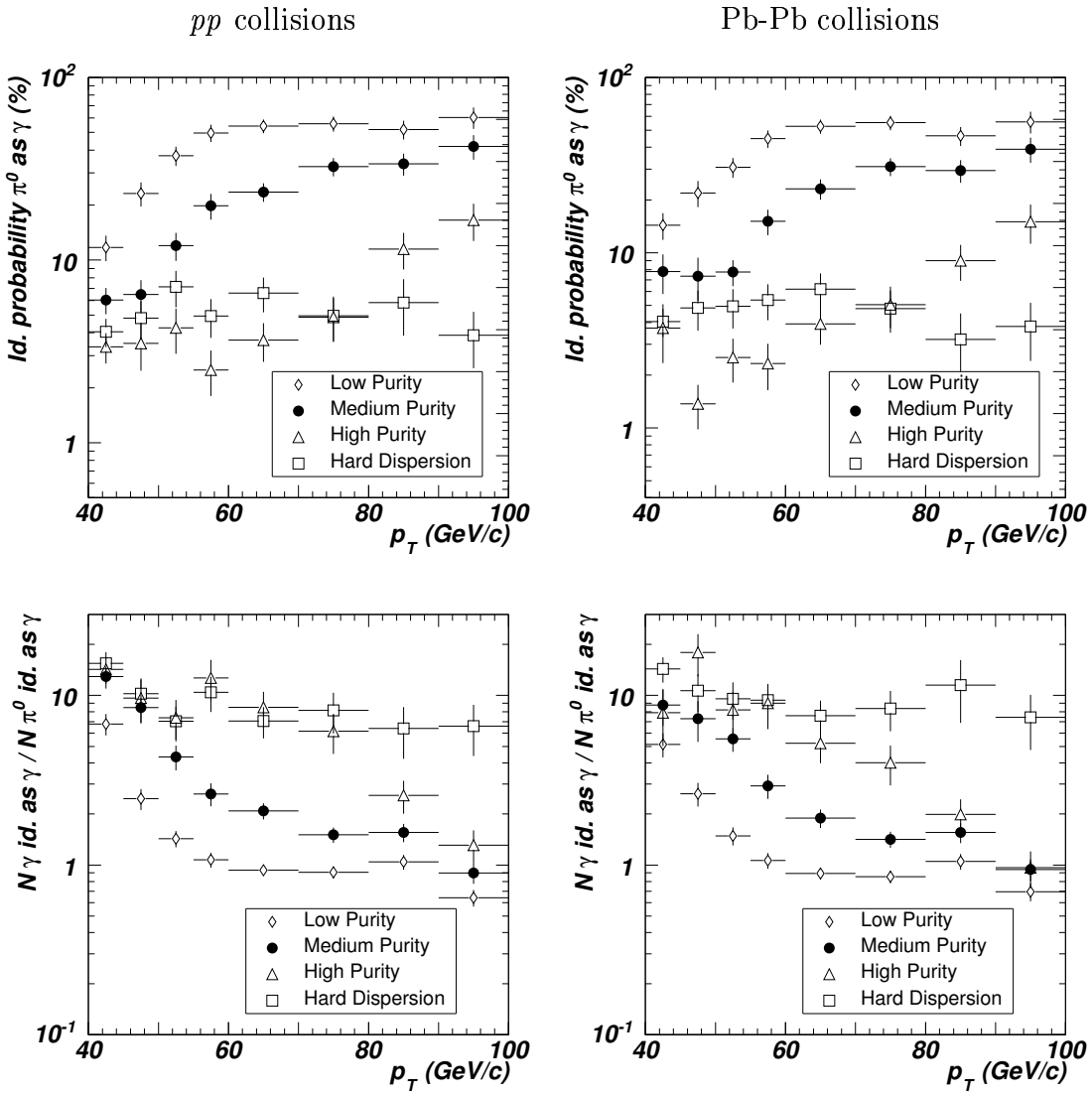

Figure 8: Upper frames: Probability to misidentify one cluster π^0 (overlapped photons) from jet-jet events detected in PHOS as photons, for pp (left) and Pb-Pb (right) collisions with shower shape analysis. Lower frames: Ratio of photons identified as photons in γ-jet events to one cluster π^0's (overlapped photons) identified as photons in jet-jet events. Only a small fraction of jet-jet events has a leading π^0 detected in PHOS, which explains the large statistical errors.

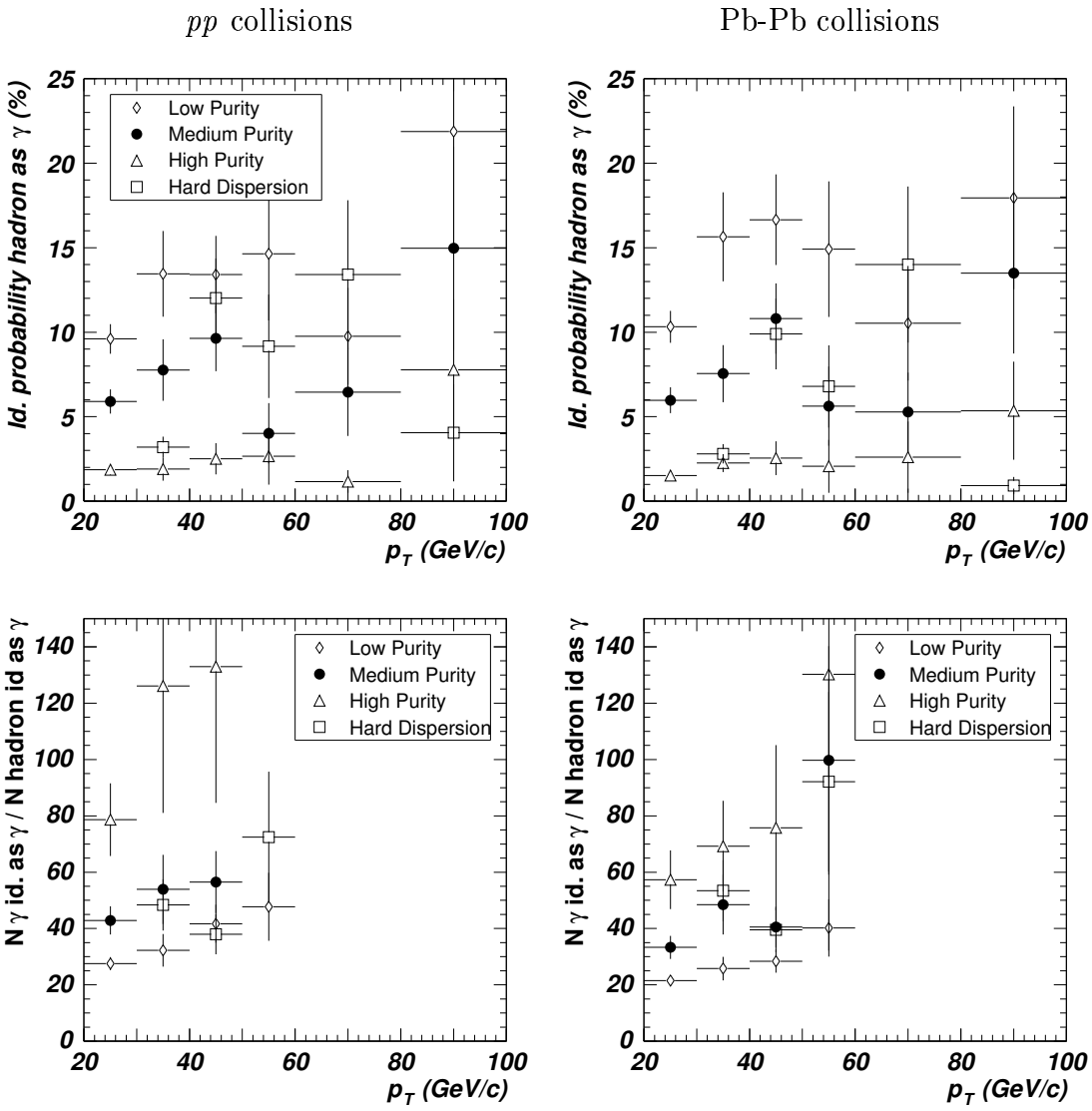

Figure 9: Upper frames: Probability to identify any charged hadron or baryon from jet-jet events detected in PHOS as photons, for pp (left) and Pb-Pb (right) collisions with shower shape analysis. Lower frames: Ratio of photons identified as photons in γ-jet events to hadrons identified as photons in jet-jet events. Only a small fraction of jet-jet events has a leading hadron detected in PHOS, which explains the large statistical errors.

R	$p_T^{th} = 2$ GeV/c	$p_T^{th} = 4$ GeV/c	$p_T^{th} = 6$ GeV/c
	pp collisions		
0.1-0.8	100 %	100 %	100 %
	Pb-Pb collisions		
0.1	83 %	98 %	100 %
0.2	50 %	93 %	98 %
0.3 - 0.8	23-0.3 %	84-34 %	95-74 %

Table 3: Ratio of isolated to all particles obtained for γ-jet events ($20 < E_\gamma < 100$ GeV) with the ICM for several p_T thresholds and cone sizes for pp and Pb-Pb collisions without considering detector response.

$$R = \sqrt{(\phi_0 - \phi)^2 + (\eta_0 - \eta)^2}. \quad (6)$$

In Fig. 10 are shown p_T distributions of the particle multiplicity (charged or neutral) inside different cone sizes in pp and Pb-Pb collisions for γ-jet and jet-jet events. The multiplicity depends on the cone size and the event type. In pp collisions, γ-jet events produce almost no particle inside the cone, independently of the energy of the prompt photons but for jet-jet events there is a clear dependence of the multiplicity with the jet energy. Thus applying p_T cuts on the particles present inside a cone around a photon candidate can help to distinguish between the type of event, γ-jet or jet-jet. Based on this idea, we have considered two different selection criteria, to declare a photon candidate isolated and tagged as a prompt photon:

1. No hadron with a p_T above a given threshold is found (standard ICM).
2. The sum of the transverse momentum of all hadrons inside the cone, $\sum_{p_T}$, is smaller than a given threshold (ICM with threshold on Sum, ICMS).

3.2.1 Isolation cut method with particle p_T threshold (ICM)

We studied the ICM efficiency for the following conditions: a cone size of $R = 0.1$, 0.2 and 0.3 and particle threshold values of $p_T^{th} = 2$, 4 and 6 GeV/c.

First we applied the method to generated events, without taking into account the detector response functions. For γ-jet events in pp collisions, the isolation efficiency (ratio of the number of candidates tagged by the ICM as prompt photon to the total number of candidates) is 100 % for any threshold value. In Pb-Pb collisions the efficiency stays constant with p_T but varies significantly with the threshold value. Table 3 shows the ICM efficiencies for γ-jet events for different R and p_T thresholds. For jet-jet events we see an important dependence with p_T and the parton energy. At low z values ($z = p_{T,i}/E_{parton}$), the efficiency is constant but close to $z = 1$, all the events are found isolated. This behaviour is expected since the larger the fragment multiplicity the more particles with low energy. Results for jet-jet events are shown for pp and Pb-Pb collisions in Figs. 11 and 12, respectively.

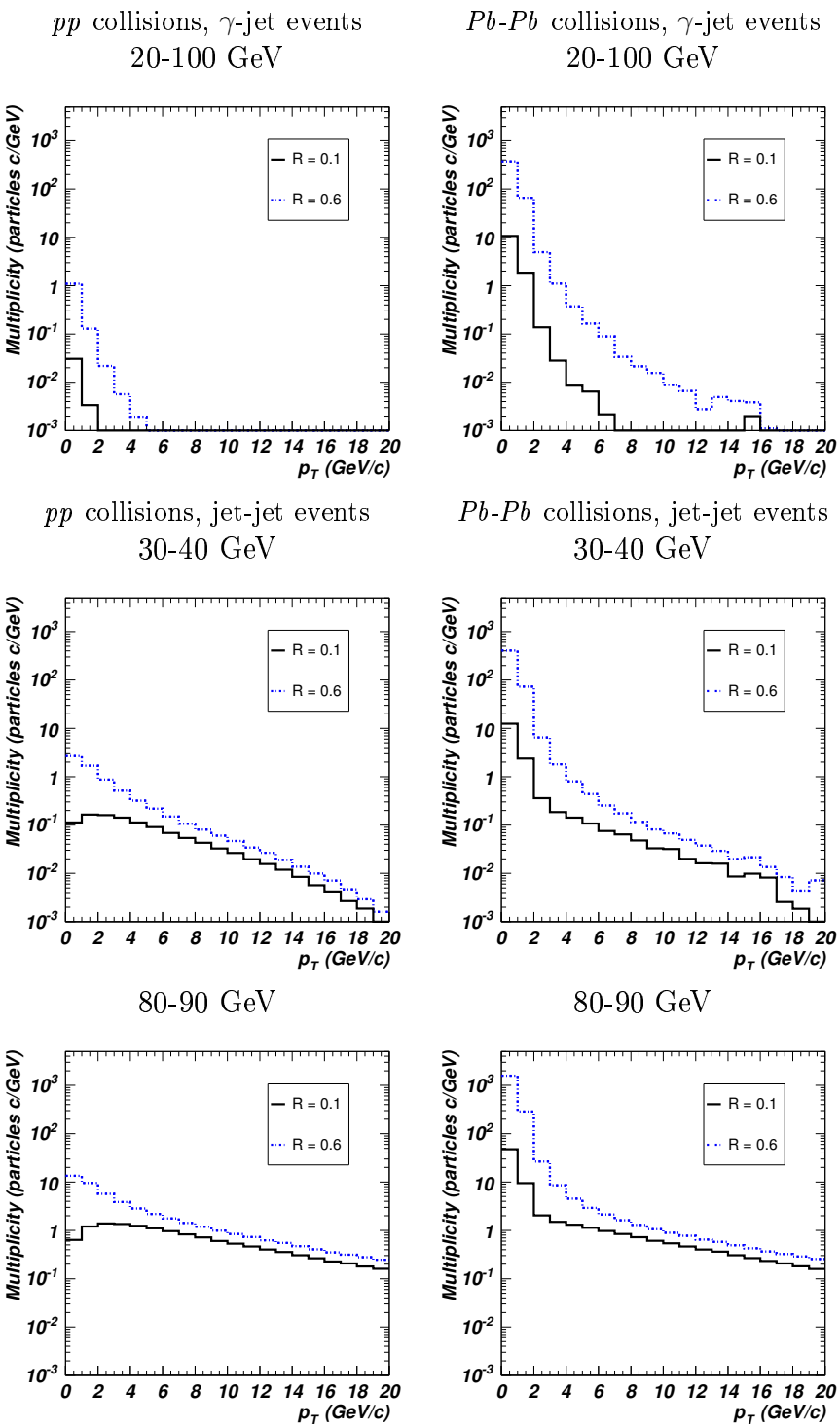

Figure 10: p_T particle distribution inside cones of size $R = 0.1$ and 0.6 around particles with p_T larger than 10 GeV/c. In these figures we show the results for generated particles, neither corrected for detector response functions nor limited to the detector acceptance. Upper figures are distributions around 20-100 GeV prompt photons (γ-jet events). Middle (30-40 GeV jets) and lower (80-90 GeV jets) figures are distributions around leading jet particles. Left figures are results for pp collisions and right ones are for Pb-Pb collisions.

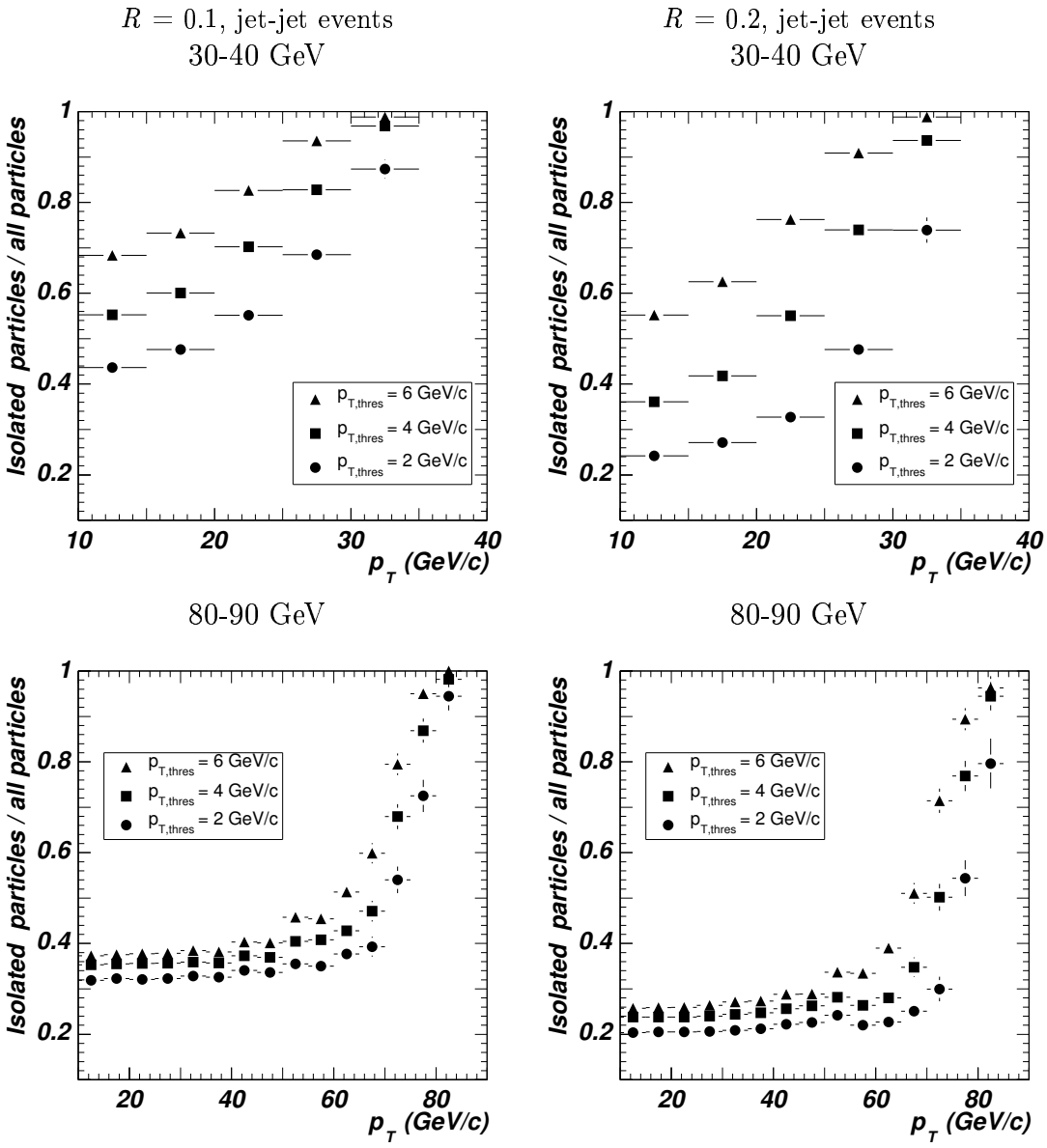

Figure 11: Ratio of isolated to all particles, depending on the particle p_T, for the ICM and several p_T thresholds in pp collisions. Two cones sizes are considered, $R = 0.1$ (left) and 0.2 (right). In these figures we show the results for generated particles, prompt photon candidates with $p_T > 10$ GeV/c, without detector response functions and without acceptance limitations. Upper figures correspond to 30-40 GeV jet-jet events and lower to 80-90 GeV jet-jet events.

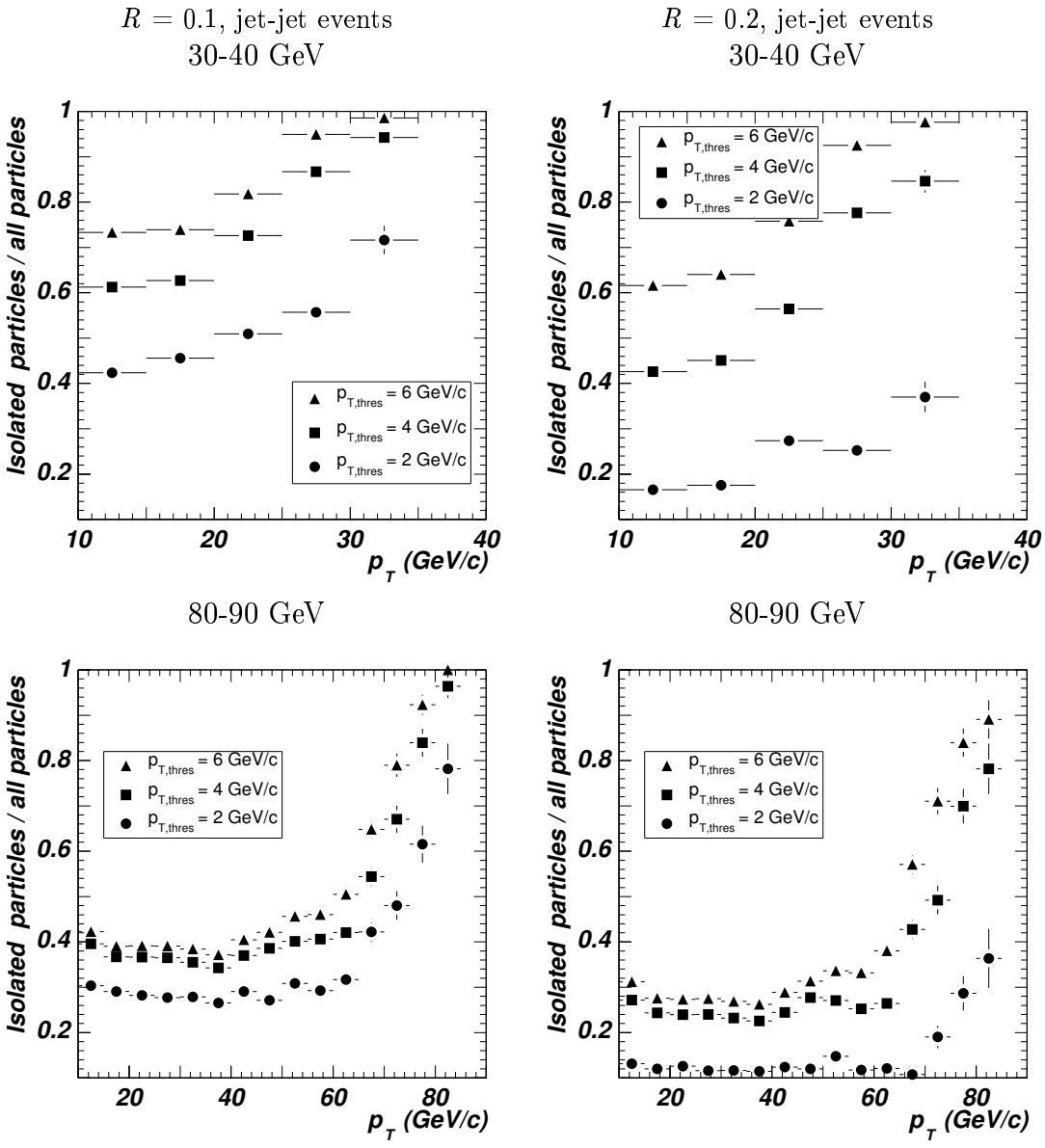

Figure 12: Ratio of isolated to all particles, depending on the particle p_T, for the ICM and several p_T thresholds in Pb-Pb collisions. Two cone sizes are considered, $R = 0.1$ (left) and 0.2 (right). In these figures we show the results for generated particles, prompt photon candidates with $p_T > 10$ GeV/c, without detector response functions and without acceptance limitations. Upper and lower figures correspond to 30-40 GeV and 80-90 GeV jet-jet events respectively.

Next, we applied the method to reconstructed events detected in the TPC and PHOS. The different jet-energy bins have been added after scaling with the corresponding cross sections. The ratio of isolated particles identified as photons by the SSA-PID (low purity) to all identified photons is constructed. The ICM efficiencies, defined as the ratio of the integral of the isolated photon spectrum to the integral of the spectrum of all photons are reported in Tab. 4 for different values of the cone size and p_T^{th}. The dependence of the efficiencies of jet-jet events with the energy of the photon candidate are shown in Fig. 13 for $R = 0.1$ and 0.2 and $p_T^{th} = 2$, 4 and 6 GeV/c. The following features are observed,

- γ-jet events: In pp collisions the ICM efficiency is close to 100 % for any momentum particle threshold, independently of the cone size and of the threshold value. At variance, in Pb-Pb collisions, there is an important dependence on both parameters, p_T^{th} and R: the bigger the cone size, the worse the isolation becomes, and the bigger the particle momentum threshold, the better the isolation efficiency becomes. No dependence with the photon energy is observed.

- jet-jet events: The ICM gives a smaller probability to identify one-cluster π^0 as photon (misidentification) in Pb-Pb than in pp collisions, the probability being larger the bigger is the particle threshold. The probability is quasi independent of the cone size for large particle momentum threshold. The dependence with the particle momentum threshold is strong, ranging from $\sim$56 % for $p_T^{th} = 6$ GeV/c to $\sim$16-20 % for $p_T^{th} = 2$ GeV/c in pp collisions and is even smaller in Pb-Pb collisions.

The signal (γ-jet) to background (jet-jet) ratios are reported in Tab. 5 and Fig. 14. In pp collisions, the ratio rises slightly with R for $p_T^{th} = 2$ GeV/c, and in Pb-Pb collisions, it shows a maximum at $R = 0.3$. For larger momentum thresholds, the dependence with R disappears and the signal to background ratio becomes smaller. The optimum value of the ICM parameters, $R = 0.2$ and $p_T^{th} = 2$ GeV/c, is deduced.

3.2.2 Isolation cut method with total p_T sum in cone threshold (ICMS)

We follow the same methodology as the one described in the previous section. The ICMS method is based on the value of the sum of the transverse momentum of all the particles entering a given cone around the photon candidate. This sum is denoted as Σ_{p_T}. In pp collisions, we have studied the efficiency of the method for threshold values of 0.7, 1, 2 and 3 GeV/c and for Pb-Pb collisions, for threshold values between 5 and 50 GeV/c. However, for Pb-Pb collisions Σ_{p_T} is not the appropriate parameter to compare results obtained for different values of the cone size because Σ_{p_T} varies significantly with R (Fig. 15). A more appropriate parameter is the momentum sum density Σ'_{p_T} defined as:

$$\Sigma'_{p_T} = \frac{\Sigma_{p_T}}{R^2 \times f(R)}, \tag{7}$$

where $f(R)$ is a factor that takes into account the response functions of the various detectors involved and their acceptance. It is equal to 1 if we do not take into

R	$p_T^{th} = 2$ GeV/c	$p_T^{th} = 4$ GeV/c	$p_T^{th} = 6$ GeV/c
	pp collisions		
	γ-jet events		
0.1 - 0.8	100 %	100 %	100 %
	jet-jet events		
0.1	20 %	42 %	56 %
0.2	16 %	41 %	56 %
0.3 - 0.8	16 %	41 %	56 %
	Pb-Pb collisions		
	γ-jet events		
0.1	80 %	98 %	99 %
0.2	50 %	95 %	99 %
0.3 - 0.8	34 - 8 %	93 - 84 %	98 - 97 %
	jet-jet events		
0.1	15 %	39 %	56 %
0.2	7 %	37 %	54 %
0.3 - 0.8	4 - 1 %	36 - 31 %	54 - 53 %

Table 4: ICM efficiency defined as the ratio of the isolated photon integrated spectrum to the photon integrated spectrum (photons previously identified with SSA-PID low purity) for reconstructed pp and Pb-Pb events in PHOS and TPC.

R	$p_T^{th} = 2$ GeV/c	$p_T^{th} = 4$ GeV/c	$p_T^{th} = 6$ GeV/c
	pp collisions		
0.1	3	1.4	1
0.2	3.5	1.4	1
0.3 - 0.8	3.6-3.7	1.4	1
	Pb-Pb collisions		
0.1	3	1.4	1
0.2	4.2	1.4	1
0.3 - 0.8	4.6 - 3	1.5	1

Table 5: ICM signal (γ-jet) to background (jet-jet) ratio: it is the ratio of the isolated photon integrated spectrum to the total photon integrated spectrum (photons previously identified with low purity) for reconstructed pp and Pb-Pb events in PHOS and TPC. R and p_T^{th} are the parameters of the ICM, the cone size and particle momentum threshold.

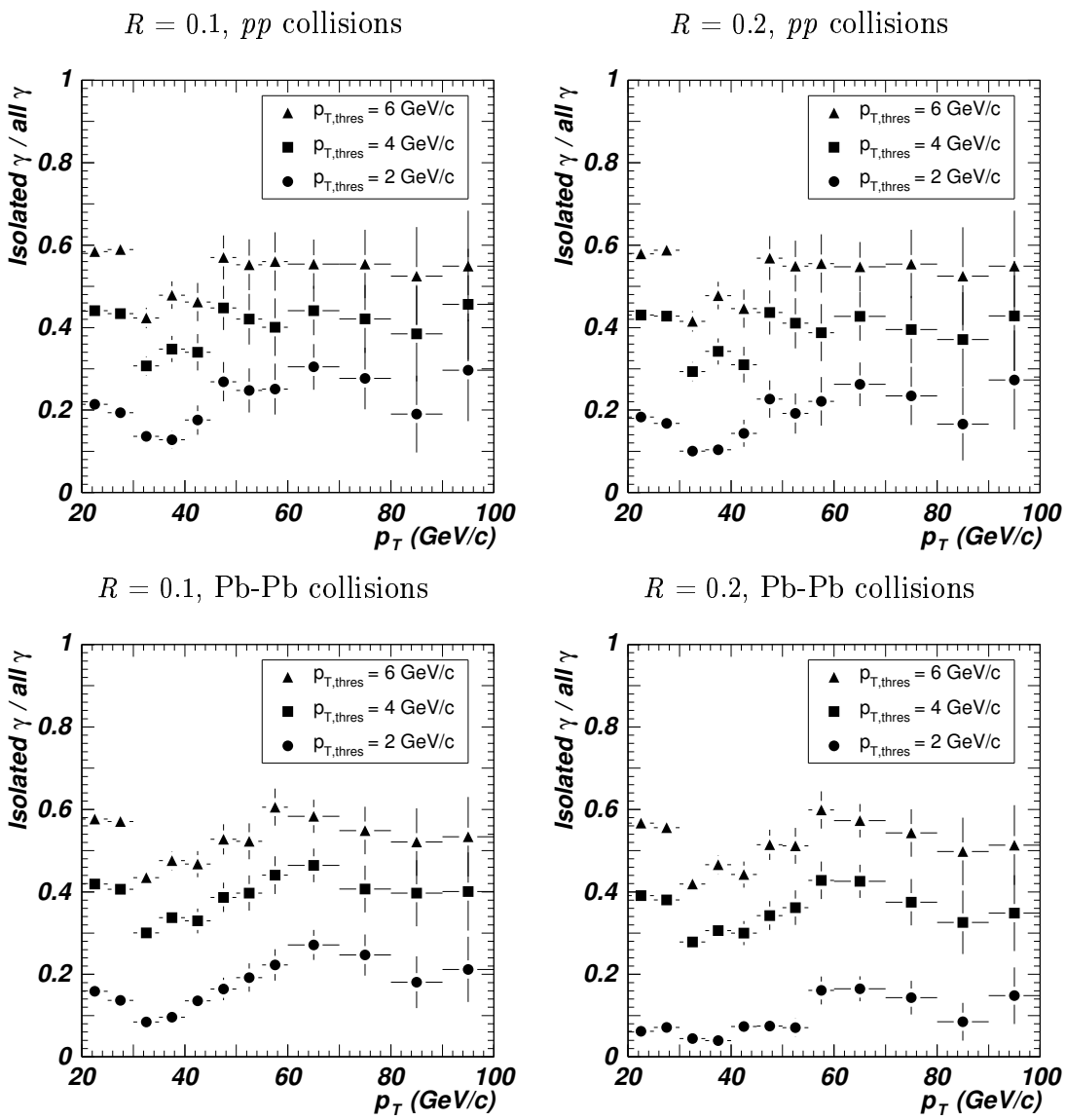

Figure 13: Misidentification efficiency of ICM identified prompt photons as function of the photon p_T for $R = 0.1$ (left) and $R = 0.2$ (right) cone sizes and 2, 4 and 6 GeV/c p_T thresholds. This efficiency is defined as the ratio of isolated photon spectrum to the total photon spectrum, being photons previously identified as low purity photons by the SSA method. Upper and lower figures show the misidentification efficiency for pp and Pb-Pb collisions respectively.

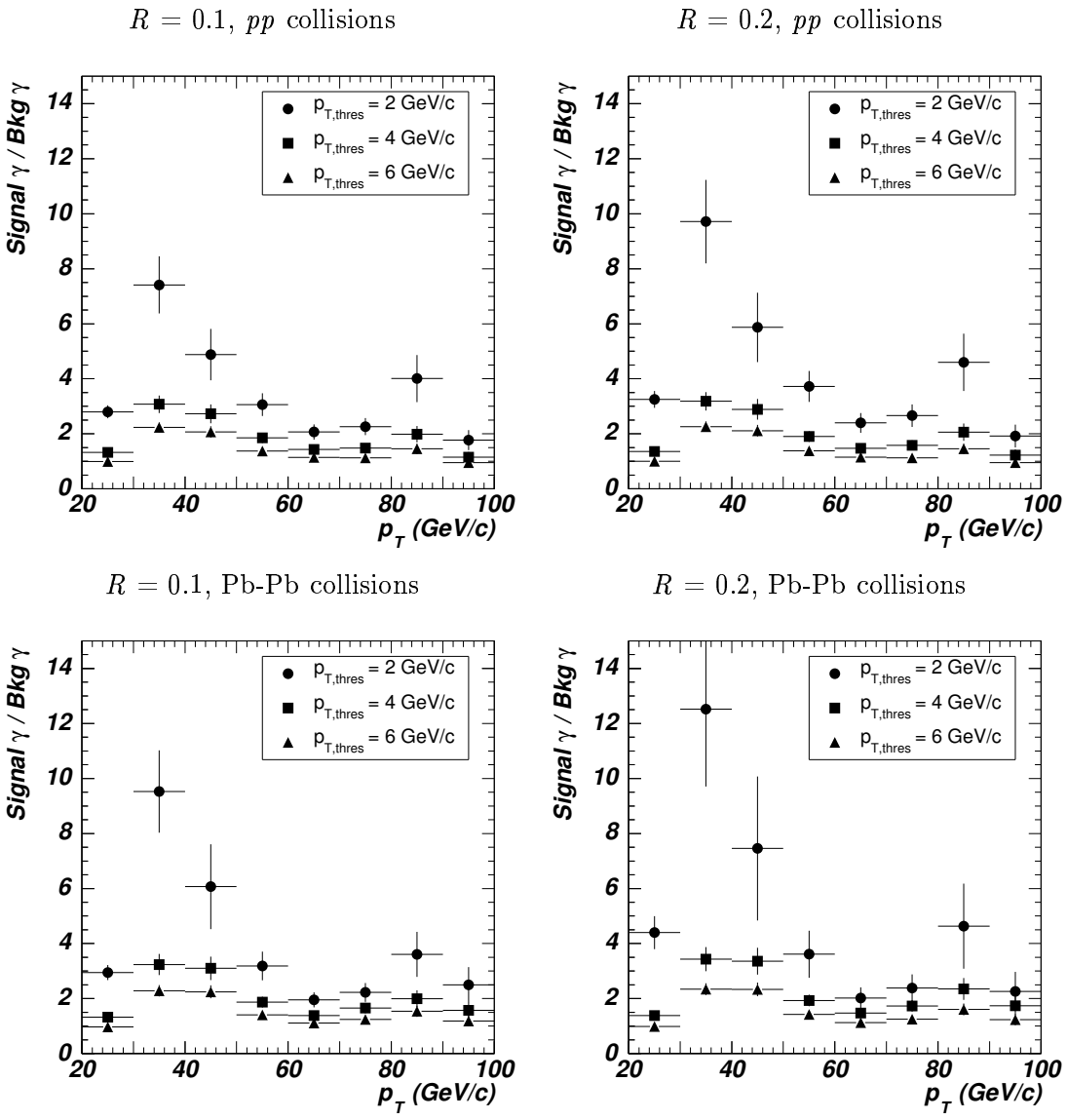

Figure 14: Signal (identified prompt photons by SSA-PID low purity and ICM fromγ-jet events) over background (identified prompt photons by SSA-PID low purity and ICM from jet-jet events) as function of p_T, for $R = 0.1$ (left) and 0.2 (right), and p_T^{th} of 2, 4 and 6 GeV/c. Upper frame: pp collisions. Lower frame: Pb-Pb collisions.

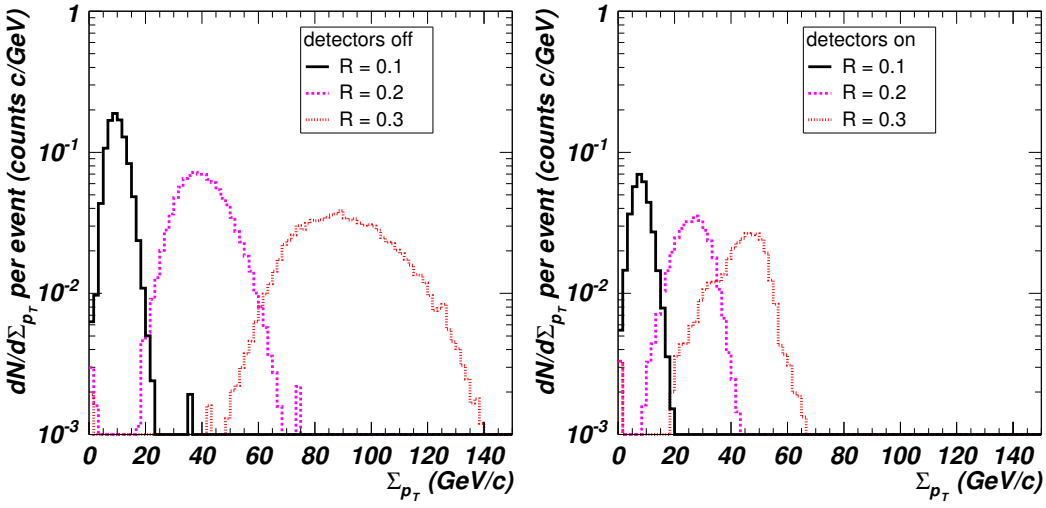

Figure 15: p_T sum of all particles inside cons sizes $R = 0.1$, 0.2 and 0.3 in a HIJING event. In the left figure we count all simulated particles (charged and neutral), the acceptance and resolution of detectors are not taken into account. In the right figure only the particles detected in the TPC (charged) and PHOS (neutral) are considered in the cone.

	$R = 0.1$	$R = 0.2$	$R = 0.3$
Generated particles	10 GeV/c	40 GeV/c	91 GeV/c
Detected particles	8 GeV/c	26 GeV/c	43 GeV/c

Table 6: Gaussian mean value of the Σ_{p_T} distribution (Figs. 15) depending on the cone size $R = 0.1$, 0.2 and 0.3, if we consider all particles of the simulation or just the detected particles.

account the detector effects and in the presence of the detector effects we take the empirical formula $f(R) = 0.95 - 1.5 \times R$, deduced from the data reported in Tab. 6.

As in the previous section, we applied the ICMS to all generated particles. We observe a similar behavior. Table 7 shows the ICMS efficiencies for γ-jet events for different R and p_T thresholds. Results for jet-jet events are shown for pp and Pb-Pb collisions in Figs. 16 and 17.

We applied the method to reconstructed events and we have constructed the ICMS efficiency, reported in Tab. 8 for different values of the cone size and Σ_{p_T} or Σ'_{p_T}. The dependence of this efficiency for jet-jet events with the energy of the photon candidate is shown in Figs. 18 for $R = 0.1$ and 0.2 and the most appropriate Σ_{p_T} and Σ'_{p_T} thresholds for each cone size,

- γ-jet events: In pp collisions the ICMS efficiency is close to 100 %, for each momentum particle threshold, independently of the cone size and of the threshold value. At variance, in Pb-Pb collisions, there is an important dependence on both parameters, R and Σ'_{p_T}: the bigger the cone size, the better the isolation efficiency becomes and the lower Σ'_{p_T}, the better the isolation efficiency

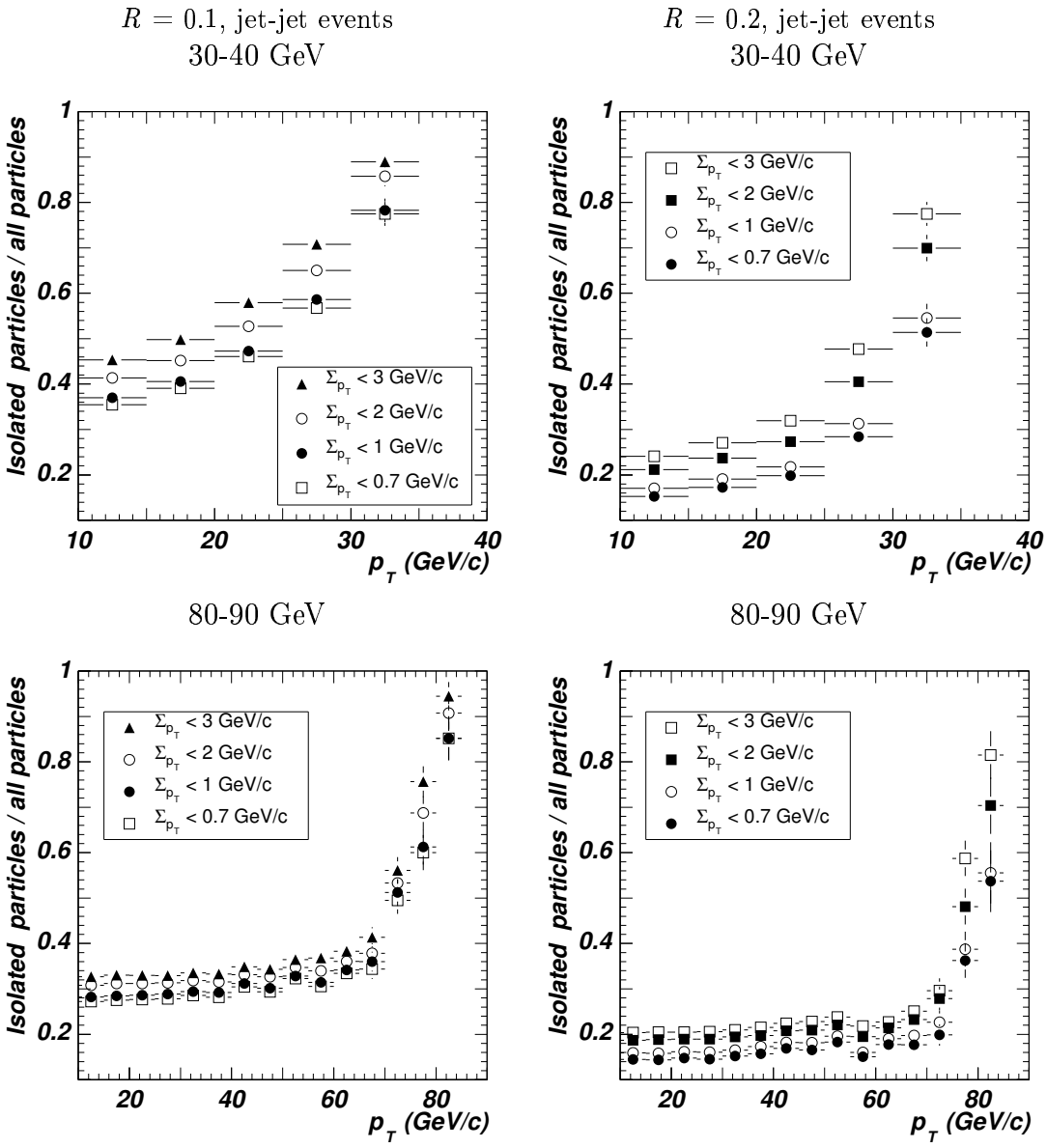

Figure 16: Ratio of isolated to all particles, depending on the particle p_T, for the ICMS and several Σ_{p_T} thresholds in pp collisions. Two cone sizes are considered, $R = 0.1$ (left) and 0.2 (right). In this figures we show the results for generated particles, prompt photon candidates with $p_T > 10$ GeV/c, without detector response functions and without acceptance limitations. Upper figures correspond to 30-40 GeV jet-jet events and lower to 80-90 GeV jet-jet events.

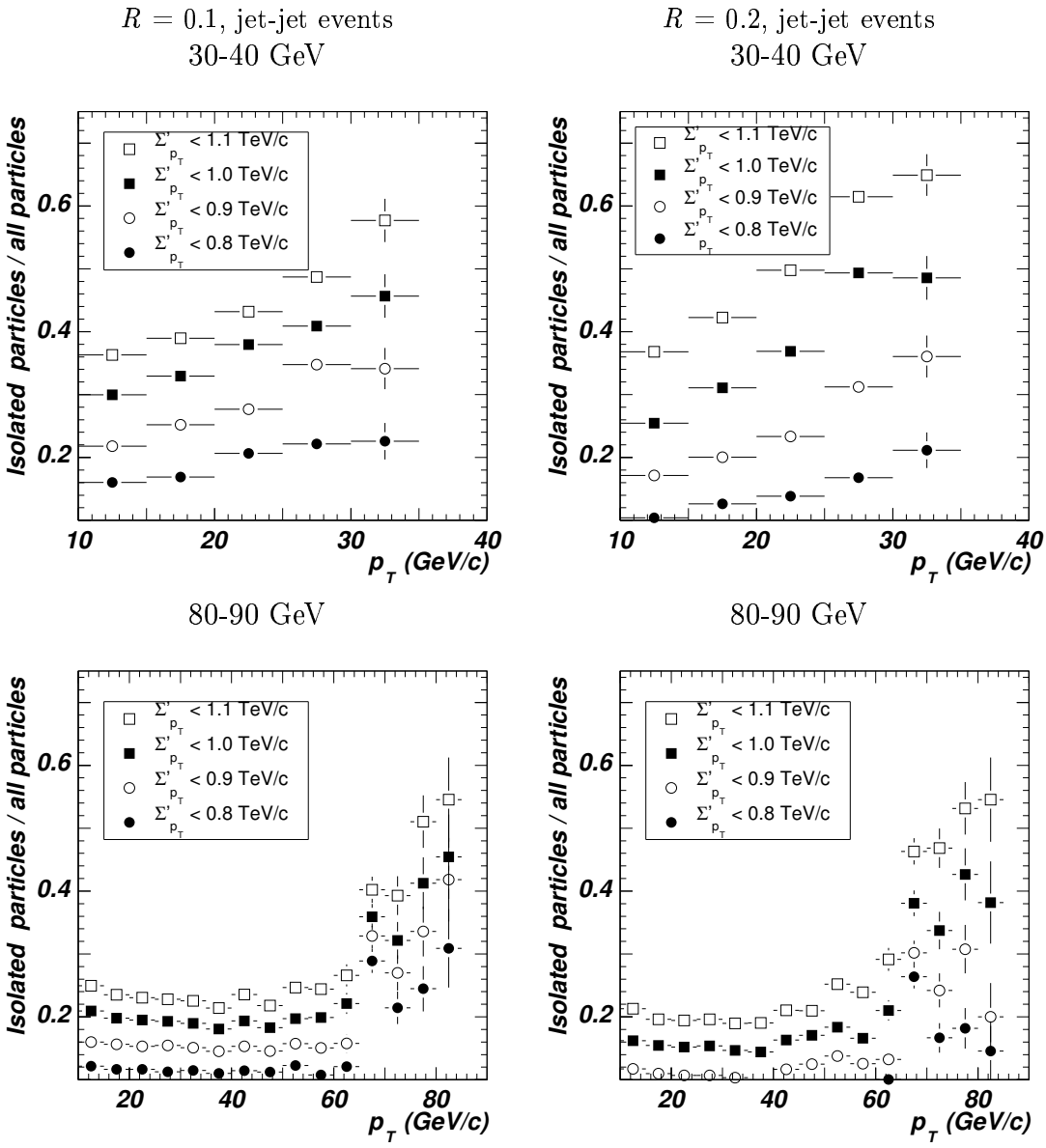

Figure 17: Ratio of isolated to all particles, depending on the particle p_T, for the ICMS and several Σ_{p_T} thresholds int Pb-Pb collisions. Two cone sizes are considered, $R = 0.1$ (left) and 0.2 (right). In these figures we show the results for generated particles, prompt photon candidates with $p_T > 10$ GeV/c, without detector response functions and without acceptance limitations. Upper and lower figures correspond to 30-40 GeV and 80-90 GeV jet-jet events, respectively.

	$R = 0.1$	$R = 0.2$
Σ_{p_T}(GeV/c)	pp collisions	
0.7	97 %	92 %
1	99 %	96 %
> 2	100 %	100 %
Σ'_{p_T}(TeV/c)	Pb-Pb collisions	
0.8	30 %	18 %
0.9	41 %	34 %
1	52 %	51 %
1.1	63 %	67 %

Table 7: Ratio of isolated to all particles obtained for γ-jet events ($20 < E_\gamma < 100$ GeV) with the ICMS method for several p_T thresholds and cone sizes for pp and Pb-Pb collisions without considering detector response.

becomes. For example for any R and $\Sigma'_{p_T} < 1$ TeV/c, the efficiency is about 50 %. No dependence with the photon energy is observed.

- jet-jet events: In pp collisions the ICMS probability to misidentify one-cluster π^0 as photon depends slightly on the cone size, and strongly on the threshold: for example, for $\Sigma_{p_T} < 1$ GeV/c the probability is about 8-4 % and for $\Sigma_{p_T} < 3$ GeV/c it is about 22-15 % in the range $0.1 < R < 0.3$. In Pb-Pb collisions, there is an important dependence on both parameters: for example, for $\Sigma'_{p_T} < 1$ TeV/c, the misidentification probability is about 12-28 % and for $\Sigma'_{p_T} < 1.2$ TeV/c, the misidentification probability is about 17-52 % in the range $0.1 < R < 0.3$. We obtain the best π^0 rejection when the threshold is small. The ICMS probability to misidentify one-cluster π^0 as photon is also almost independent of the photon candidate p_T.

The signal (γ-jet) to background (jet-jet) ratios are reported in Tab. 9 and Fig. 19. In pp collisions, the ratio rises with R and decreases as Σ_{p_T} increases. In Pb-Pb collisions, the ratio decreases with R and shows a small dependence on Σ'_{p_T}, with a maximum at $\Sigma'_{p_T} \sim 1$ TeV/c. The optimum value of ICMS parameters is deduced from this pattern: for pp collisions, the optimum values are $R = 0.2$ and $\Sigma_{p_T} < 0.7$ GeV/c (the ratio is better for $R = 0.3$ but we prefer to take the same cone sizes 0.1 or 0.2 like in the previous section) and for Pb-Pb collisions, we obtain the best signal to background ratio for $R = 0.1$ and $\Sigma'_{p_T} < 0.9$ TeV/c.

3.2.3 Comparison between the two ICM methods

By comparing the signal to background ratios obtained with both methods we can conclude the following:

- For pp collisions, a threshold on Σ_{p_T} is more efficient as the jet-jet events are more suppressed ($R = 0.2$ and $\Sigma_{p_T} < 0.7$ GeV/c, γ-jet efficiency 100 %, jet-jet misidentification 5 %), than a simple p_T threshold selection ($R = 0.2$ and $p_T^{th} = 2$ GeV/c, γ-jet efficiency 100 %, jet-jet misidentification 20 %).

pp collisions			
$\Sigma_{p_T}(\mathrm{GeV}/c)$	$R = 0.1$	$R = 0.2$	$R = 0.3$
	γ-jet events		
any	100 %	100 %	100 %
	jet-jet events		
0.7	6.1 %	3.2 %	2.1 %
1.0	7.9 %	4.5 %	3.8 %
2.0	15 %	10 %	8.6 %
3.0	22 %	16 %	15 %
Pb-Pb collisions			
$\Sigma'_{p_T}(\mathrm{TeV}/c)$	$R = 0.1$	$R = 0.2$	$R = 0.3$
	γ-jet events		
0.7	18 %	11 %	14 %
0.8	28 %	21 %	24 %
0.9	36 %	34 %	36 %
1.0	48 %	49 %	54 %
1.1	56 %	62 %	73 %
1.2	64 %	77 %	92 %
	jet-jet events		
0.7	4.8 %	5.8 %	8.3 %
0.8	7.2 %	9.1 %	14 %
0.9	8.5 %	15 %	20 %
1.0	12 %	20 %	28 %
1.1	15 %	25 %	37 %
1.2	17 %	35 %	52 %

Table 8: ICM efficiency defined as the ratio of the isolated photon spectrum integral to the total photon spectrum integral (photon previously identified with SSA-PID low purity) for reconstructed pp and Pb-Pb events in PHOS and TPC.

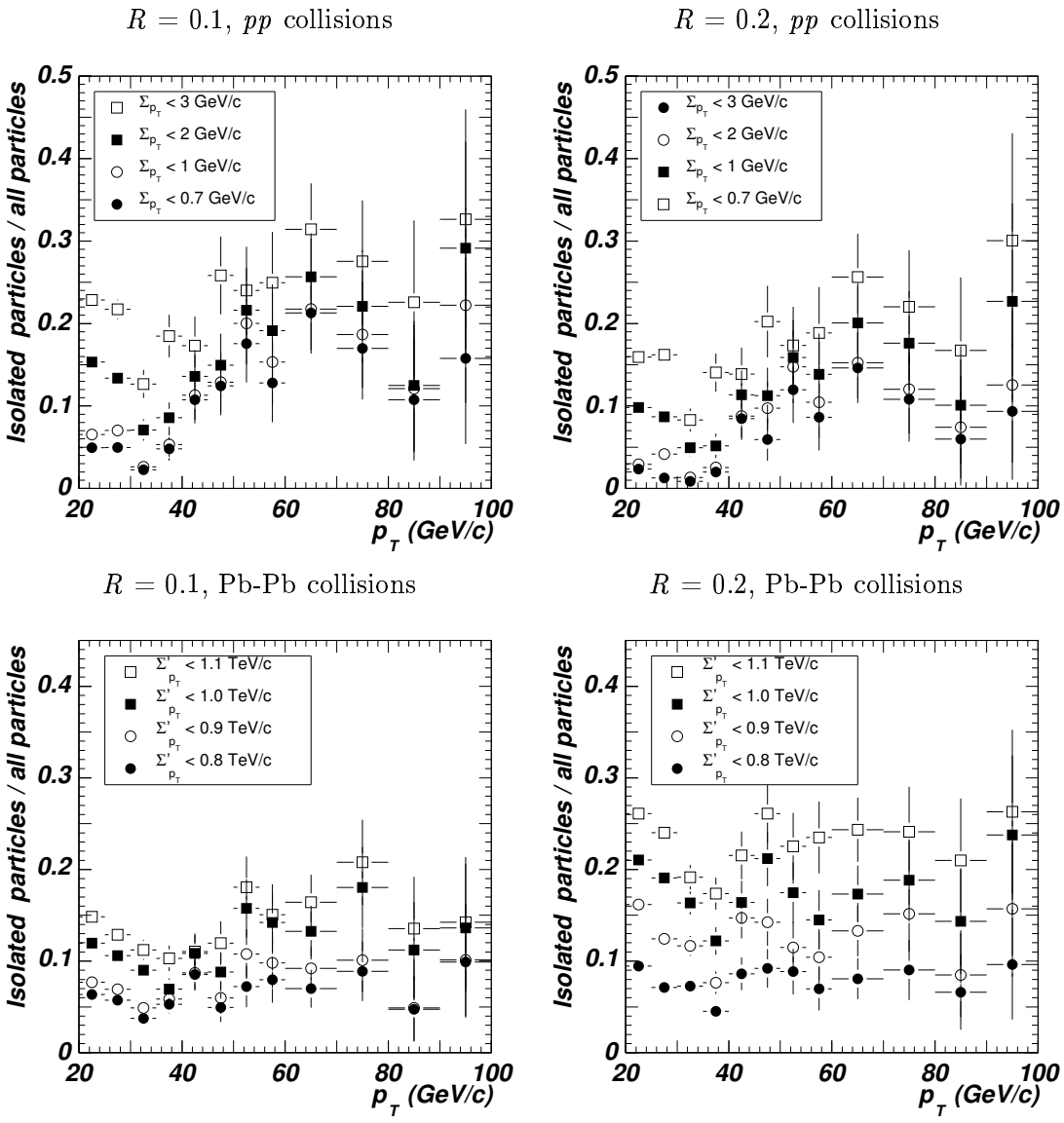

Figure 18: Misidentification efficiency of ICMS identified prompt photons as a function of the candidate p_T for $R = 0.1$ (left) and $R = 0.2$ (right), $\Sigma_{p_T} = 0.7$, 1, 2 and 3 GeV/c per cone size unity for pp collisions (upper figures) and $\Sigma'_{p_T} = 0.8$, 0.9, 1 and 1.1 TeV/c per cone size unity for Pb-Pb collisions (lower figures).

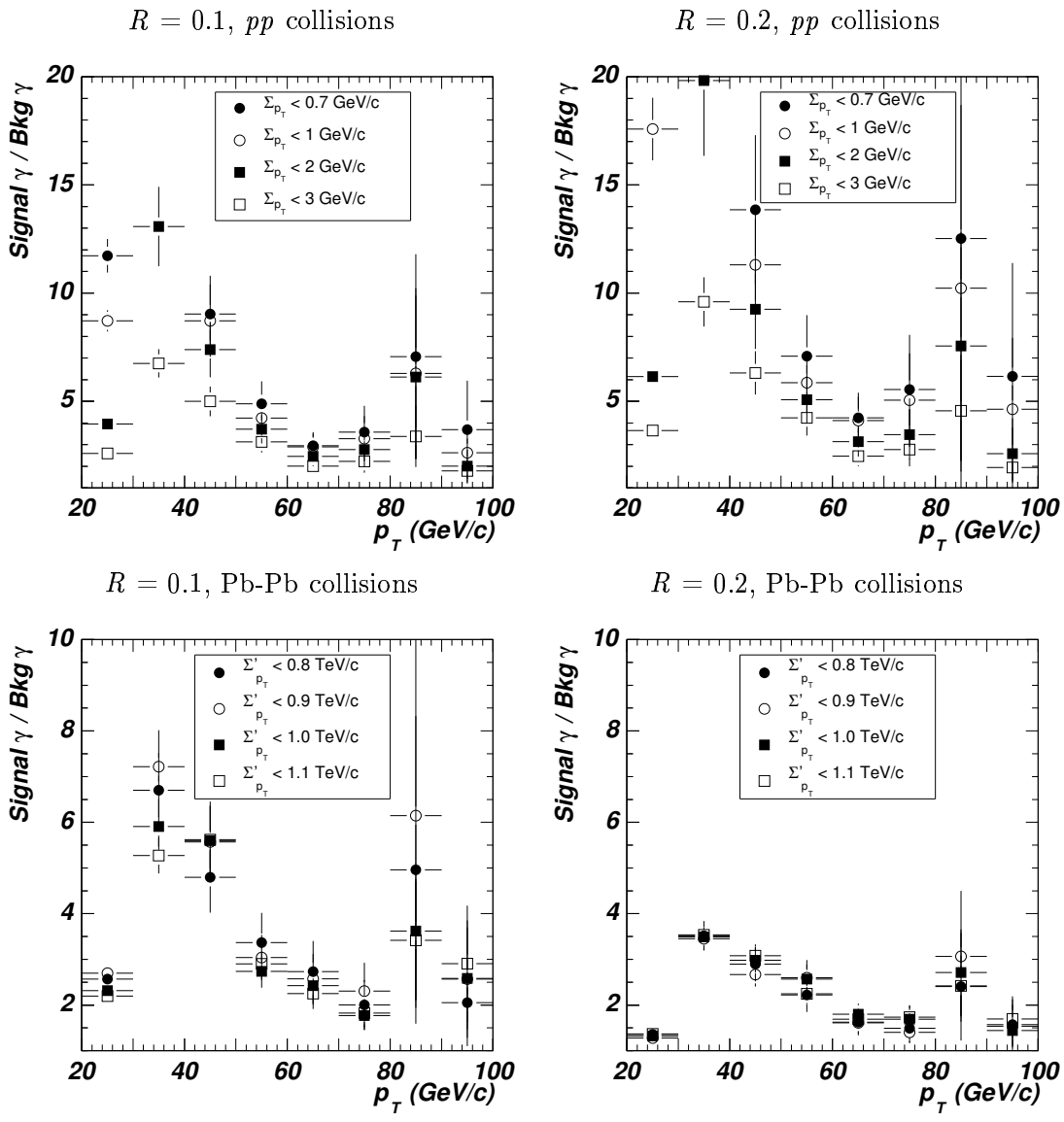

Figure 19: Signal (identified prompt photons by SSA-PID low purity and ICM fromγ-jet events) over background (identified prompt photons by SSA-PID low purity and ICM from jet-jet events) as function of p_T, for $R = 0.1$ (left) and 0.2 (right), and $\Sigma_{p_T} = 0.7$, 1, 2 and 3 GeV/c for pp collisions (upper frame) and $\Sigma'_{p_T} = 0.8$, 0.9, 1 and 1.1 TeV/c per cone size unity for Pb-Pb collisions (lower frame).

Σ_{p_T}(GeV/c)	$R = 0.1$	$R = 0.2$	$R = 0.3$
	pp collisions		
0.7	9.5	18	27
1.0	7.4	13	15
2.0	4.0	5.8	6.8
3.0	2.6	3.6	4.0
Σ'_{p_T}(TeV/c)	$R = 0.1$	$R = 0.2$	$R = 0.3$
	Pb-Pb collisions		
0.7	2.2	1.1	0.97
0.8	2.3	1.3	0.99
0.9	2.4	1.3	1.0
1.0	2.2	1.4	1.1
1.1	2.2	1.4	1.1
1.2	2.1	1.3	0.99

Table 9: ICMS signal (γ-jet) to background (jet-jet) ratio of the isolated photon integrated spectrum to the total photon integrated spectrum (photons previously identified with SSA-PID low purity) for reconstructed *pp* and Pb-Pb events in PHOS and TPC.

- For Pb-Pb collisions, at variance, a threshold on the particle p_T gives a better identification efficiency ($R = 0.2$ and $p_T^{th} = 2$ GeV/c, γ-jet efficiency 50 %, jet-jet misidentification 7 %) than the optimum condition reached with the Σ_{p_T} threshold scheme ($R = 0.1$ and $\Sigma'_{p_T} < 0.9$ TeV/c, γ-jet efficiency 36 %, jet-jet misidentification 8.5 %).

The final identified prompt photon spectrum obtained after applying the ICM methods (Fig. 20) is compared to the spectrum obtained after applying SSA-PID (Fig. 6): we conclude that a sufficiently important background rejection is achieved. It has been observed at RHIC that the hadron spectrum is quenched by a factor 5 [22]. Assuming such a value, the jet-jet contribution would be lowered by the same factor (Fig. 20-right), leading to a signal to background ratio of 20 instead of 4 (for $R = 0.2$ and $p_T^{th} = 2$ GeV/c, see Tab 5).

3.3 Final particle spectrum

We construct the final prompt photon spectrum, as it will be measured during one running period and calculate the statistical and systematic errors. We add the identified-photon spectrum from γ-jet events with the ones from jet-jet events, to obtain the total identified-photon spectrum, N_γ^{id}. Knowing the identification probabilities, we can reconstruct the original spectrum in the following way. Let N_γ be the original prompt photon spectrum, N_{π^o} the original π^o spectrum and N_h the original hadron spectrum, and ε_i^j the corresponding particle identification as photon (PID) or prompt photon (ICM) efficiencies, then

$$N_\gamma^{id} = N_\gamma \varepsilon_\gamma^{pid} \varepsilon_\gamma^{icm} + N_{\pi^o} \varepsilon_{\pi^o}^{pid} \varepsilon_{\pi^o}^{icm} + N_h \varepsilon_h^{pid} \varepsilon_h^{icm},$$

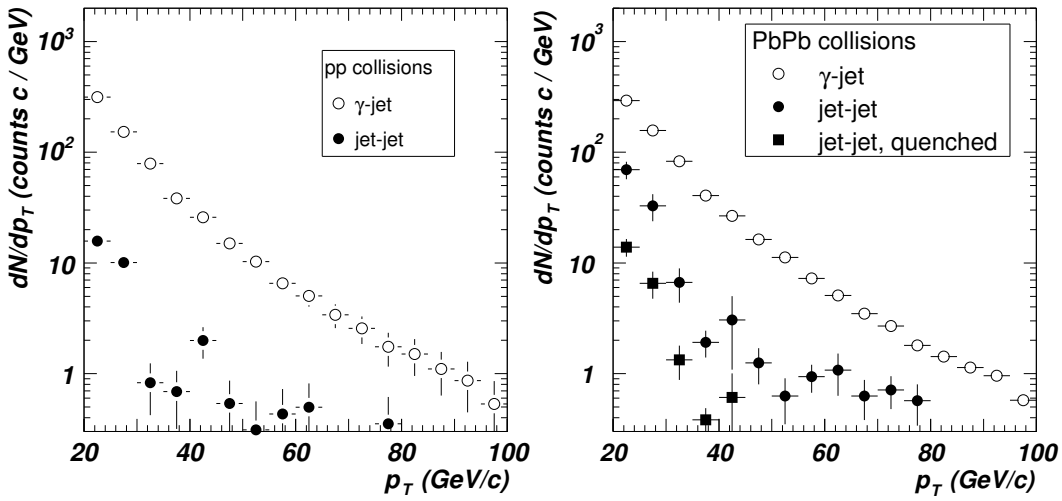

Figure 20: Spectra of prompt photons identified in ALICE during a LHC running year with statistical errors by SSA-PID medium purity and ICMS (pp) and ICM (Pb-Pb) for jet-jet and γ-jet events in pp (left) and Pb-Pb (right) collisions at $5.5A$ TeV. In Pb-Pb collisions, we assumed a quenching factor of 5 to γ-like events.

$$N_\gamma^{id} = N_\gamma(\varepsilon_\gamma^{pid}\varepsilon_\gamma^{icm} + \frac{N_{\pi^0}}{N_\gamma}\varepsilon_{\pi^o}^{pid}\varepsilon_{\pi^o}^{icm} + \frac{N_h}{N_\gamma}\varepsilon_h^{pid}\varepsilon_h^{icm}) = \zeta N_\gamma.$$

From the studies discussed in the previous sections, we deduce the various factors (the misidentification efficiency of ICM for π^o and hadrons is the same) and construct the correction factor ζ for the different identification criteria (PID photon classes, cone sizes and p_T thresholds). The PID systematic errors were calculated as the dispersion around the average of the corrected spectra obtained with the different identification criteria. This dispersion is added quadratically with the average background spectra to obtain the total systematic error. The statistical error is calculated as $\sqrt{N_\gamma^{id}}$.

The final spectra of identified photons are shown in Fig. 21, together with the comparison to the original spectra. In Fig. 22, we assume that hadrons produced in Pb-Pb collisions are quenched by a factor 5 as observed at RHIC. This reduces the systematic error.

4 γ-jet identification

To identify photon-jet events we proceed as follows:

1. Search in each event for the most energetic prompt photon identified in PHOS.

2. Search for the leading particle[9] associated to the highest p_T value, in the same

[9]Jets have always some particles that can carry a significant proportion of the jet energy (in average 40%).

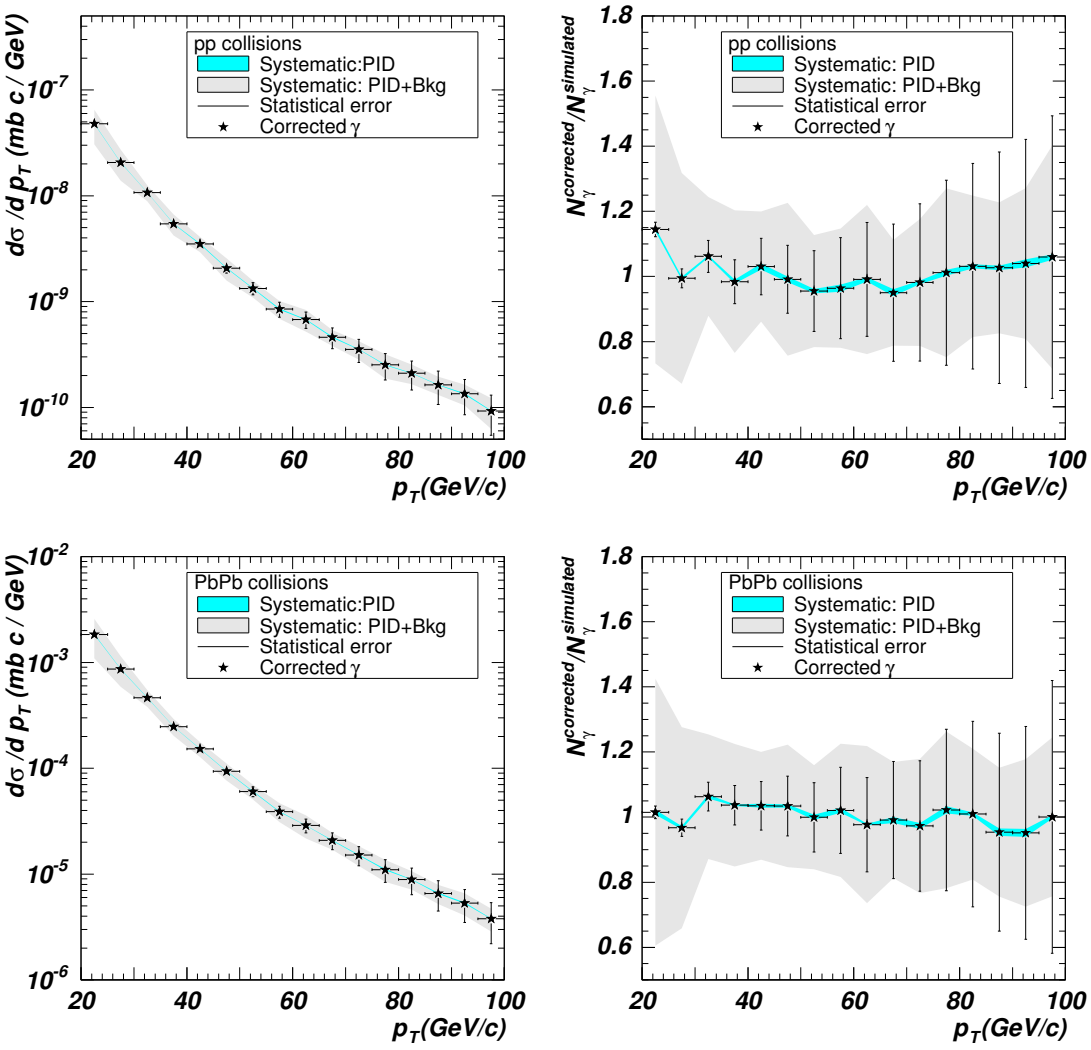

Figure 21: Left frames: Final prompt photon spectrum obtained after the correction of the different identified spectra, shown with statistical and systematical errors due to identification and background (jet-jet events). Right frames: Ratio of the corrected prompt photon spectrum and the original simulated spectrum. Results are presented for both *pp* (up) and Pb-Pb (down) collisions at 5.5A TeV.

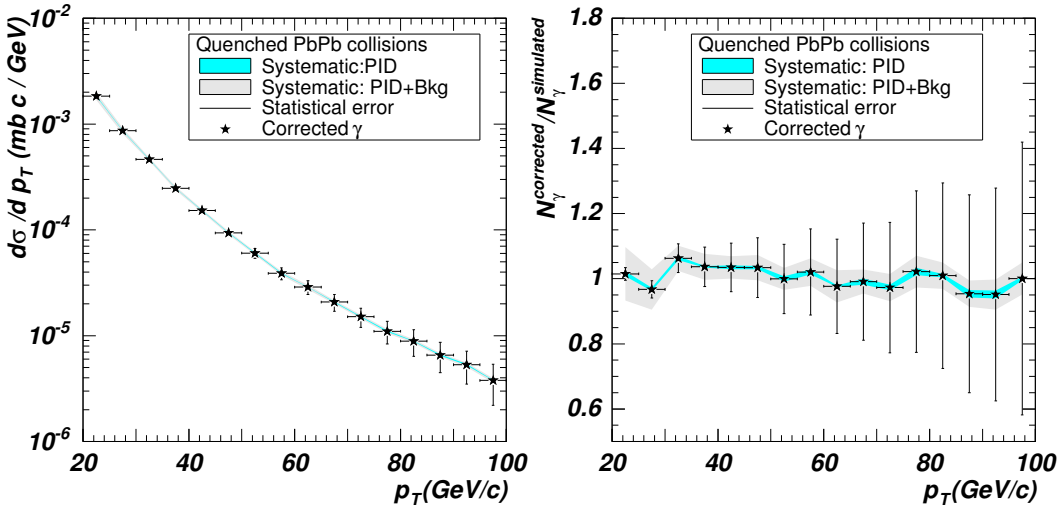

Figure 22: We assume a quenching factor of 5 reducing the hadrons spectrum in Pb-Pb collisions at 5.5A TeV. Left frame: Final prompt photon spectrum obtained after the correction of the different identified spectra, shown with statistical and systematical errors due to identification and background (jet-jet events). Right frame: Ratio of the corrected prompt photon spectrum and the original simulated spectrum.

event, according to the following criteria :

(a) detected by the central tracking system ($|\eta| < 0.7$) or the EMCal (see Tab. 1).

(b) charged or neutral (π^0). In the latter case it will decay into two photons and we consider all the photon pairs in the event (see Sec. 4.2) whose:

i. relative angle is between a maximum and minimum angle defined by the decay kinematics ,

ii. the invariant mass must satisfy, $120 < M_{\gamma\gamma} < 150$ MeV/c^2.

(c) emitted almost back-to-back to the photon, i.e. with $\Delta\phi$ close to 180^o (see Sec. 4.1).

(d) its p_T value must amount to at least 10 % of the photon energy (see Sec. 4.3).

3. Reconstruct the jet as the ensemble of all particles contained inside a cone, defined by Eq. (6), whose axis is aligned along the leading particle direction. We considered $R = 0.3$ and p_T threshold values of 0.5 (2.0) GeV/c for pp (Pb-Pb) collisions (see Sec. 4.3). Finally, the event is identified as a photon-jet event if the reconstructed jet energy is comparable to the photon energy.

4.1 Aspects of γ- jet selections

Since jet particles can be collected only if they are inside the central tracking system and EMCal acceptance, only a fraction of jet particles is detected. In such a

situation, the jet energy will then be only partially reconstructed and such a jet candidate is rejected.

Since the prompt photon and the parton are emitted in opposite directions in their center of mass, the jet and the photon directions should be correlated in azimuthal and axial angles. However, the high momentum components of the parton structure function boosts the momentum of initial parton-parton pair along the beam axis leading to a misalignment in the axial direction, or equivalently, in pseudorapidity (Fig. 23). The azimuthal angle being Lorentz invariant, the correlation in azimuthal angle is conserved in the laboratory system. The relative azimuthal angle ($\Delta\phi$) is peaked at 180° and its width depends on the detector acceptance, detector resolution and energy of the event. On the contrary, there is no correlation in η. Our algorithm selects photon-leading particle pairs satisfying the condition $0.9\,\pi < \Delta\phi < 1.1\,\pi$.

If the leading particle escapes out of the detector acceptance, the algorithm finds a wrong leading particle. Such a misidentification induces a peak at low values of the $p_{T,l}/E_\gamma$ ratio (Fig. 24), where $p_{T,l}$ and E_γ are the momentum of the found leading particle and the energy of the photon, respectively. Such fake leading particles are rejected by imposing the condition $p_{T,l}/E_\gamma > 0.1$. This selection added to the previous selections reduces the jet selection probability to about 50 %, a value imposed only by the limited acceptance of the ALICE central tracking system.

4.2 Detection of π^0 as leading particles

A π^0 candidate as leading particle is identified by detecting the two decay photons in EMCal and imposing cuts in the $\gamma\gamma$ invariant mass about its rest mass. Unfortunately the $M_{\gamma\gamma}$ distributions, in particular in Pb-Pb collisions (Fig. 25), exhibit a huge combinatorial background. A stricter selection is then called for and it is based on further kinematic conditions.

The opening angle between two photons from a π^0 decay is given, in the lab system, by:

$$\cos\theta_{12} = \frac{\gamma_\pi^2\beta_\pi^2 - \gamma_\pi^2\alpha^2 - 1}{\gamma_\pi^2(1-\alpha^2)} \tag{8}$$

where α is the decay asymmetry, γ, the Lorentz factor and β the π^0 velocity. The opening angle is minimum for symmetric decays ($\alpha = 0$). By comparing (Fig. 26) the decay kinematics of simulated π^0 with the kinematics of all pairs of photons identified in Pb-Pb collisions, we can define an empirical maximum opening angle given by:

$$\theta_{max} = 0.4\ e^{-0.25\ E} + 0.025 - 2\ 10^{-4}\ E \tag{9}$$

which selects most of the decay photons and rejects most of the uncorrelated photon pairs. The aspect of calculated $M_{\gamma\gamma}$ (Fig. 26) for all the photon pairs and restricted with the opening angle selection, illustrates the power of this cut to help reduce the combinatorial background. This is however not sufficient. The final π^0 identification is performed with a selection within a $M_{\gamma\gamma}$ range about the π^0 rest mass, i.e. $120 < M_{\gamma\gamma} < 150$ MeV/c^2. The efficiency of the invariant mass selection can be estimated from the ratio of the number of decay photons from simulated π^0 to the one of

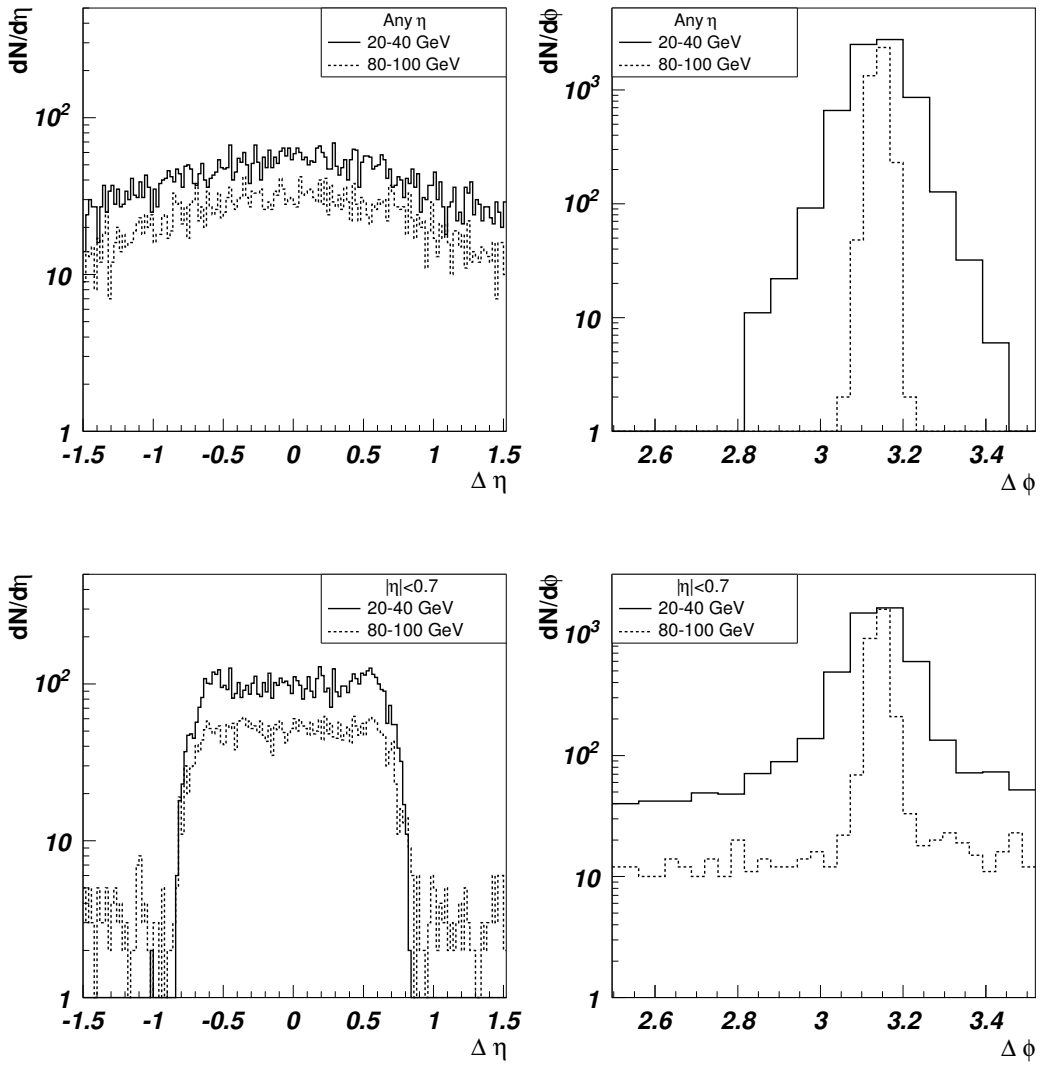

Figure 23: Angular correlations between the prompt photon and the leading particle as functions of $\Delta\eta = \eta_l - \eta_\gamma$ (left) and $\Delta\phi = \phi_l - \phi_\gamma$ (right), for simulated 20-40 GeV and 80-100 GeV γ-jet pairs in pp collisions. The detector acceptance, $|\eta| < 0.7$, has been applied to the jet particles in lower figures.

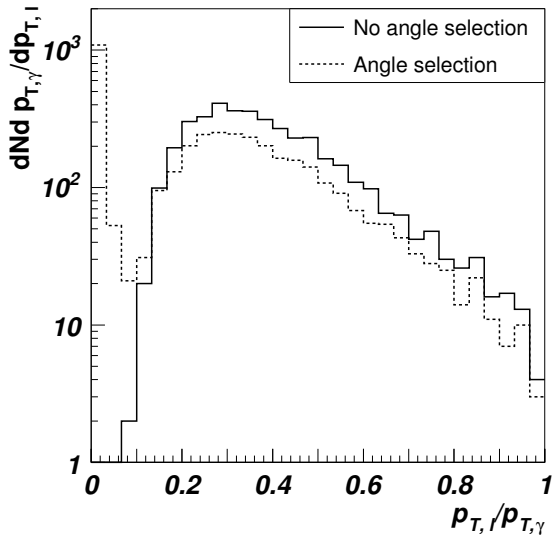

Figure 24: Particle distribution as a function of the $p_{T,l}/E_\gamma$ ratio, for pp collisions and jet energies in the range 80-100 GeV. The dotted line shows the selected leading particles that fall inside the η acceptance of the detectors, and are opposite in ϕ angle to the prompt photon. The solid line shows the leading particles without angular restriction.

all photon pairs in the heavy-ion event after the previously described selections (opening angle and leading particle). This ratio is shown in Fig. 27 and it is about 1-1.2 for energies greater than 5 GeV in pp collisions and greater than 10 GeV for Pb-Pb collisions. The ratio can be greater than one as the opening angle cut is quite restrictive, and we can lose some real pairs. We see that there is still some combinatorial background at low energies.

4.3 Jet reconstruction

The jet is reconstructed starting from the leading particle as a seed. Particles found in a cone, defined by Eq. (6), around the leading particle are assigned to the jet if their transverse momentum surpasses a given threshold. Again, we may lose a fraction of jet particles due to the limited acceptance. Therefore, only jets whose reconstructed energy is comparable to the prompt photon energy, are finally selected.

In our jet finding algorithm, two experiment configurations are considered,

- Charged particles in the central tracking system and neutral particles in EMCal (labelled TPC+EMCal in figures);
- only charged particles in the central tracking system (labelled TPC).

We compare in Fig. 28 the reconstructed jet transverse momentum, $p_{T,j}$, with the energy of the prompt photon, E_γ, for pp collisions and for various photon energies. We apply a p_T threshold of 0.5 GeV/c. In the TPC+EMCal case, the jet energy is well reconstructed as it is nearly equal to the energy of the prompt photon. In

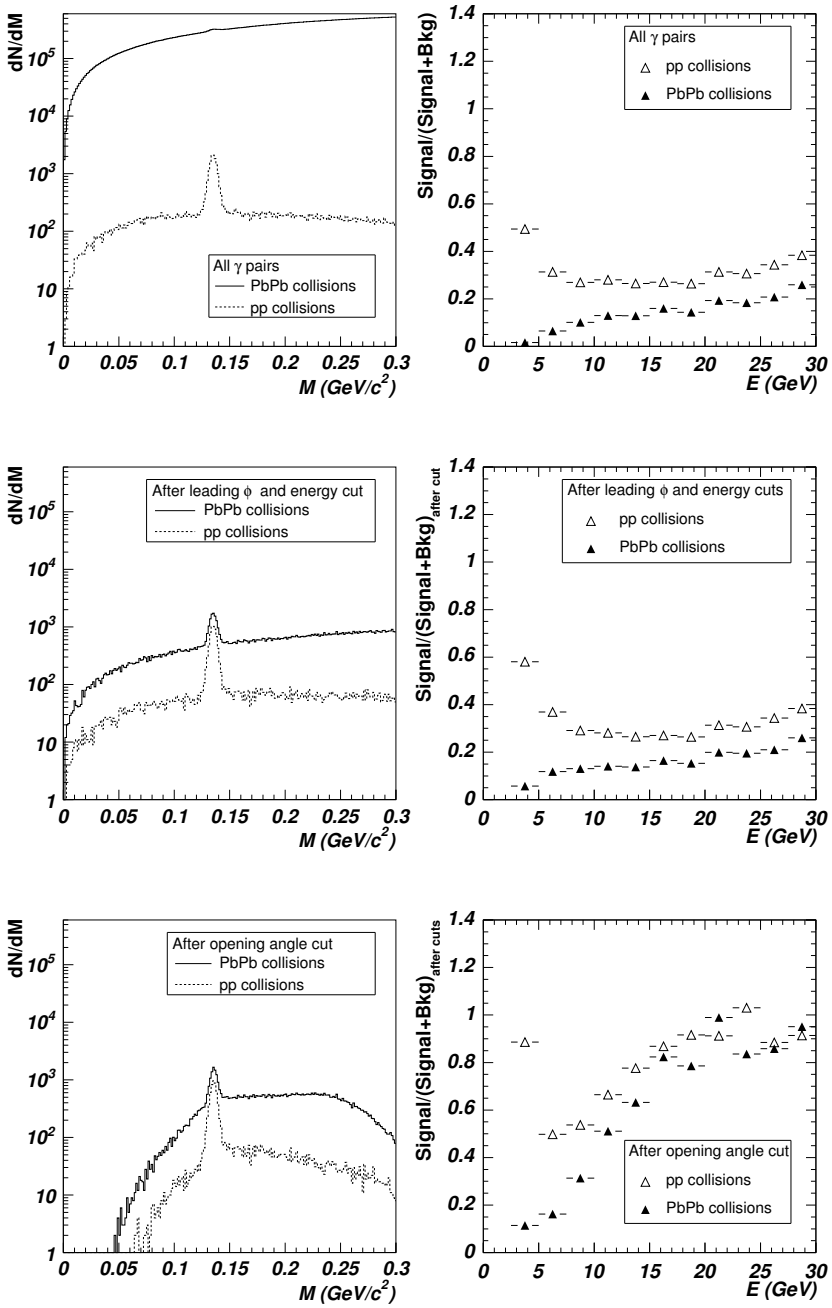

Figure 25: Left frames: Invariant mass distributions, of all possible photon pairs in the event (upper), of those pairs that have passed the ϕ correlation and the leading energy cut (middle) and when besides the pair opening angle is restricted (lower), for pp (dashed line) and Pb-Pb (solid line) collisions at $5.5A$ TeV. Right frames: Ratio of simulated signal (π^0) to the selected photon pairs in the event following the selection order of the left frames, for pp ($\triangle$) and Pb-Pb ($\blacktriangle$) collisions at $5.5A$ TeV. Figures shown for γ-jet events with energy from 20 to 100 GeV.

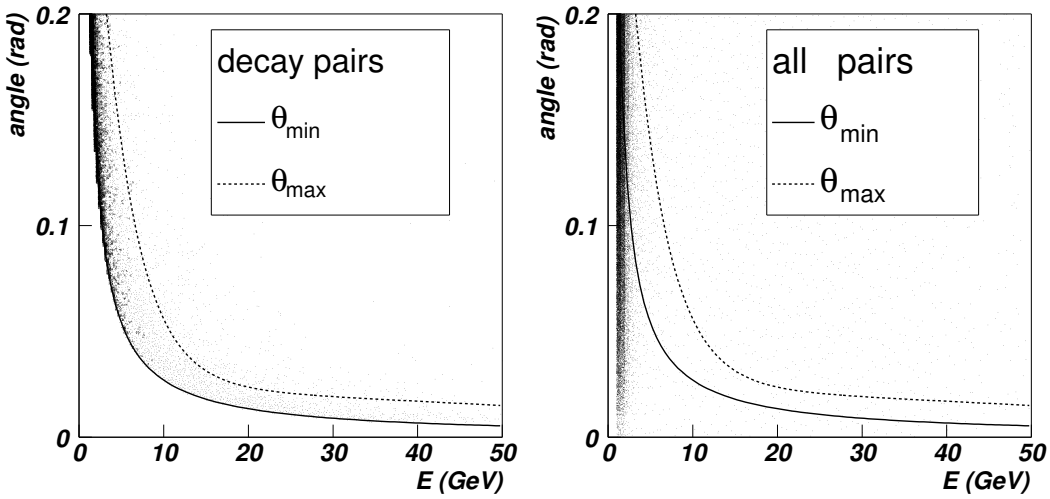

Figure 26: Relative angle of photon pairs as a function of their energy for γ-jet events in simulated Pb-Pb collisions within the energy window 80-100 GeV. Left: Opening angles of the π^0 decay photon pairs (no restriction in detector acceptance). Right: Relative angle of all photons pairs, any possible combination (only pairs inside the detectors). The lines delimit the regions where the opening angle is expected to be, the lower line is obtained from the decay kinematics, the upper one has been empirically chosen to select most of the real pairs.

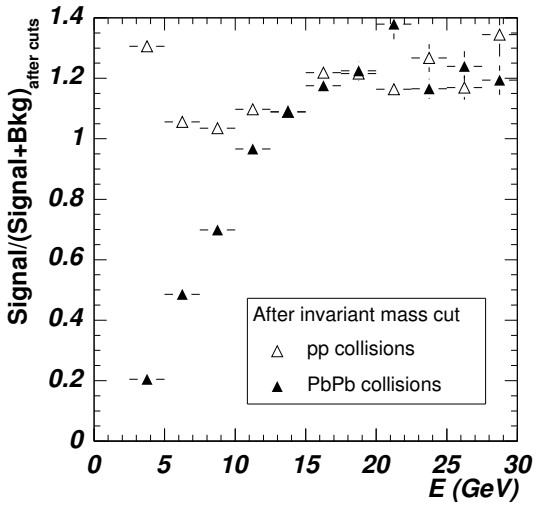

Figure 27: Ratio of simulated signal (π^0) to all photon pairs that pass the selection cuts for leading particles, the opening angle selection, and the invariant mass cuts for pp ($\triangle$) and Pb-Pb ($\blacktriangle$) collisions at $5.5A$ TeV. Figure shown for γ-jet events with energy from 20 to 100 GeV.

the absence of EMCal, the energy carried away by neutral particles is undetected. Consequently, the $p_{T,j}/E_\gamma$ distribution is rather flat. The jet reconstruction is better for higher jet energies. The result is independent of the cone size.

In Pb-Pb collisions, the background is very important and the distributions become wider and peak at values greater than one (see Fig. 29). We need to apply a higher p_T threshold to remove as much background as possible. With a threshold $p_T > 2$ GeV/c, the distribution features (peak position and width; see Fig. 30) resemble the ones obtained for *pp* collisions, at least at high jet energies. In the case of a 20 GeV/c jet the width is still large, but by imposing a higher threshold (2 GeV/c is already the 10 % of the jet energy), we risk losing too much information about the jet. Consequently we will systematically apply a p_T threshold of 0.5 GeV/c for *pp* collisions and of 2 GeV/c for Pb-Pb collisions in the investigation of jet properties (the selected cone size is 0.3). Nevertheless to construct fragmentation functions, in the next sections, we consider all detected particles inside the cone.

A photon-jet event observed with the configuration with EMCal, is perfectly identified if the the ratio $p_{T,j}/E_\gamma$ is about one. We shall consider two values for the lower limits, depending on the experimental configurations, with or without EMCal. Depending on the energy of the reconstructed jet we empirically define the selection gates of Fig. 31.

The jet reconstruction algorithm will fail for low p_T jets, as the jet signature ($p_{T,j}/E_\gamma \sim 1$) suffers large fluctuations (Fig. 32) . We have therefore excluded jets with p_T values below 10 GeV/c in our investigation.

4.4 Jet selection efficiency and contamination

The jet selection efficiency is defined by the number of identified γ-tagged jets compared to the number of prompt photons found in PHOS (see Fig. 33, upper figures, for both *pp* and Pb-Pb collisions). The efficiency for the configuration with EMCal is 30 %. For the configuration without EMCal we obtain an efficiency of 40-50 %, which is larger because of the wider selection range but implies lower identification quality.

To estimate the contamination level we have also applied the γ-jet algorithm to jet-jet events. Jets reaching PHOS may contain decay photons which, when misidentified as prompt photons, can provide the seed for the algorithm. By comparing the expected rate of hard photons identified in PHOS and originating either from γ-jet or jet-jet events (Fig. 2), we observed that the contribution of γ-like particles was comparable and often larger than the one of prompt photons. If we apply the γ-tagging algorithm to jet-jet events we can reject a substantial fraction of misidentified prompt photons. In the case of the configuration with EMCal (Fig. 33, lower frames), only about 10 % of the jet-jet events pass the selection but this value in the absence of EMCal raises to 40-50 % (*pp* and Pb-Pb collisions).

We can study the purity, $\mathcal{P}$ and contamination $\mathcal{C}$ of our selections. We define purity as the fraction of γ-jet events over the total number of identified events by our method. On the contrary, the contamination is defined as the fraction of jet-jet events over the total number of identified events, i.e. $\mathcal{C} = 1 - \mathcal{P}$. In the case of the TPC+EMCal configuration, the application of our selection criteria leads to a

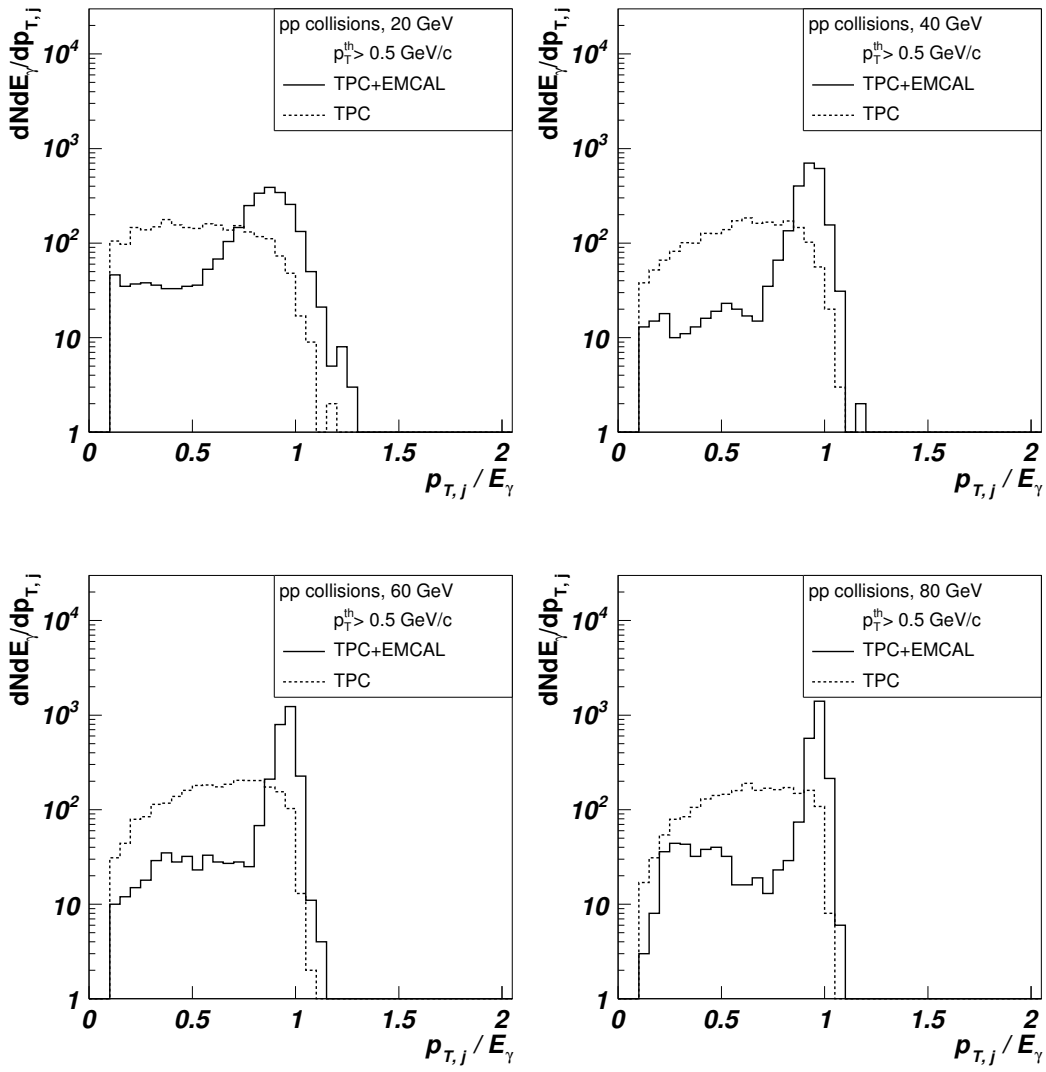

Figure 28: Jet distribution as a function of the ratio $p_{T,j}/E_\gamma$ for jets of different energy. Results for pp simulations are shown. A jet cone with $R = 0.3$ has been considered in all cases. There is a jet particle threshold of $p_T > 0.5$ GeV/c. In each sub-figure the results for two experimental configurations are given: without EMCal (dashed line) and with EMCal (solid line).

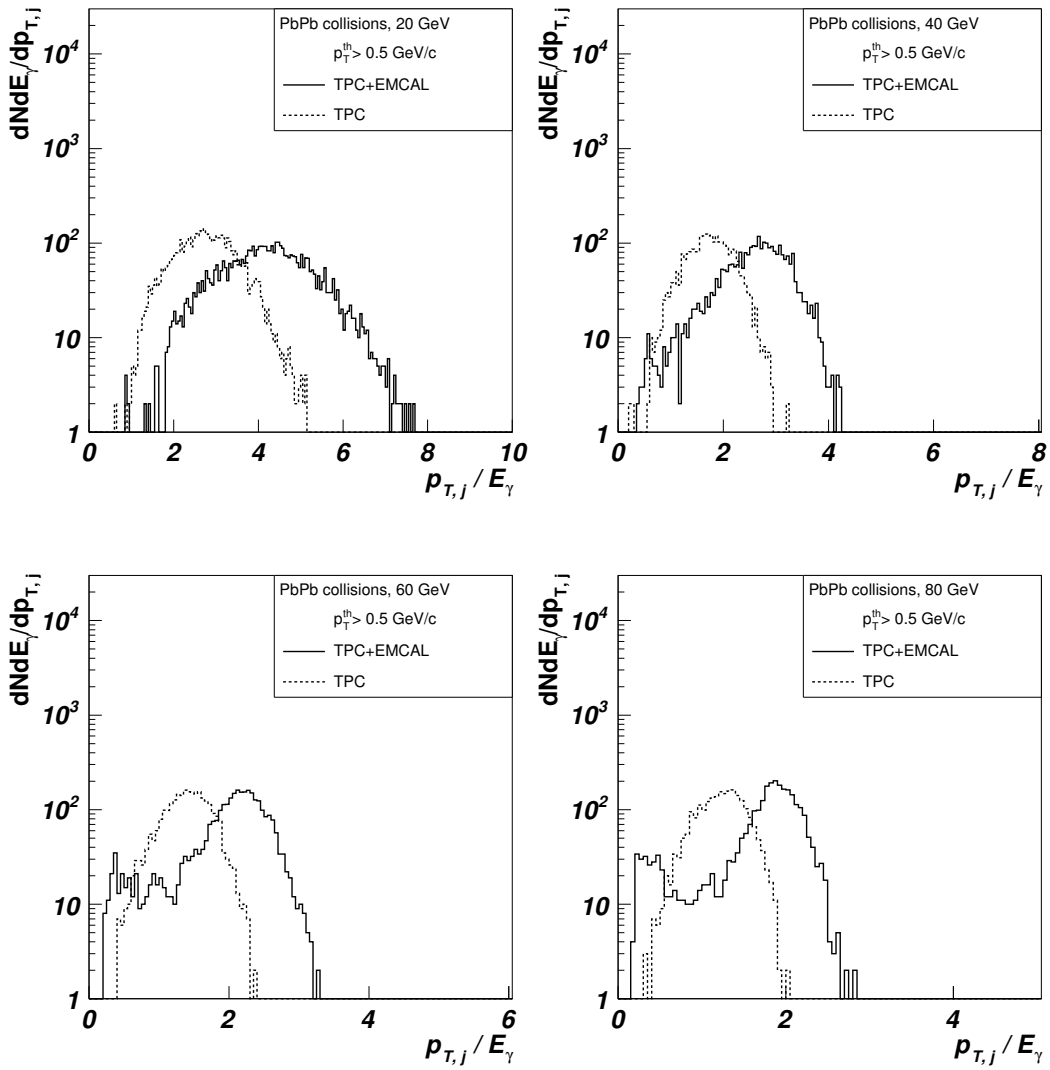

Figure 29: Jet distribution as a function of the ratio $p_{T,j}/E_\gamma$ for jets of different energy. Results for Pb-Pb simulations are shown. A jet cone with $R = 0.3$ has been considered in all cases. There is a jet particle threshold of $p_T > 0.5$ GeV/c. In each sub-figure the results for two experimental configurations are given: without EMCal (dashed line) and with EMCal (solid line).

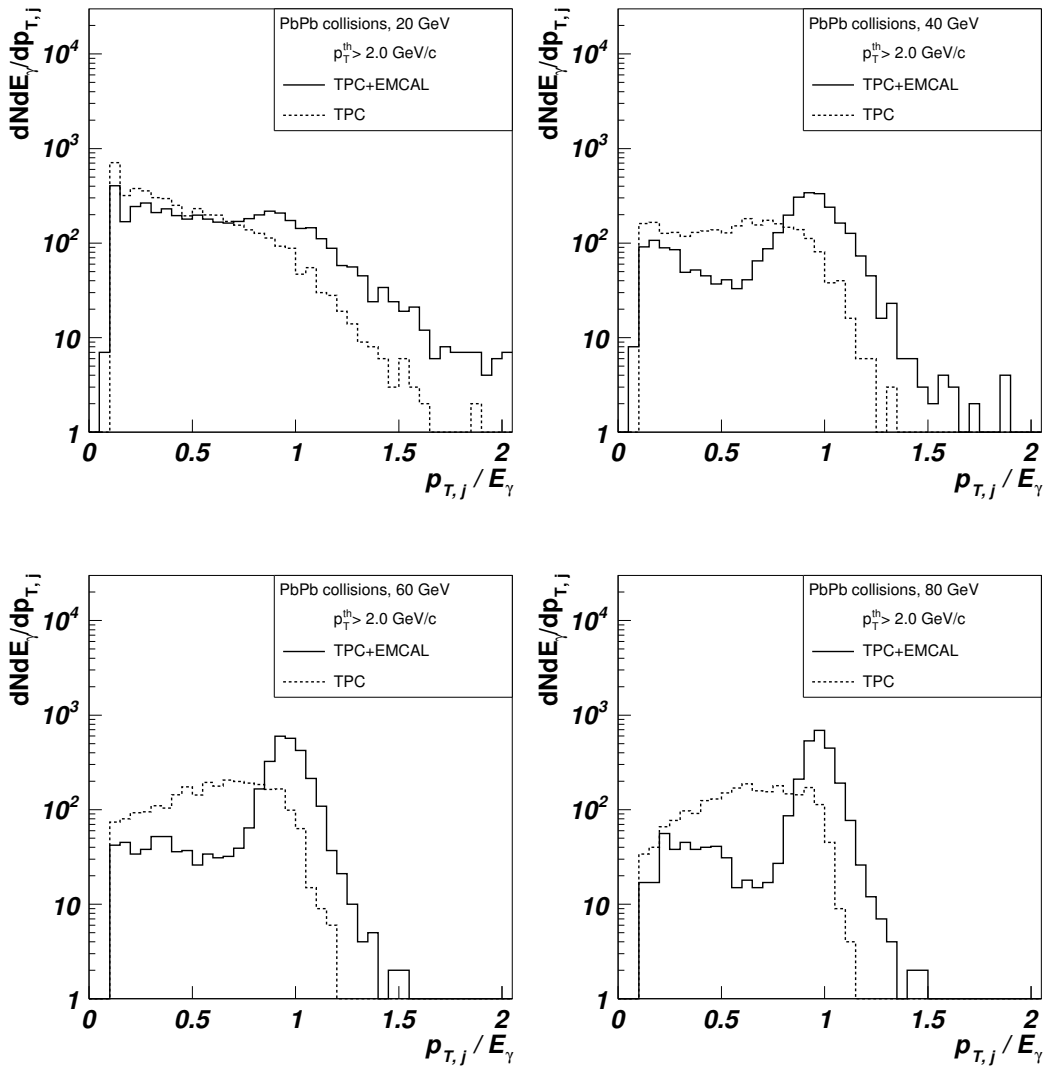

Figure 30: Jet distribution as a function of the ratio $p_{T,j}/E_\gamma$ for jets of different energy. Results for Pb-Pb simulations are shown. A jet cone with $R = 0.3$ has been considered in all cases. There is a jet particle threshold of $p_T > 2$ GeV/c. In each sub-figure the results for two experimental configurations are given: without EMCal (dashed line) and with EMCal (solid line).

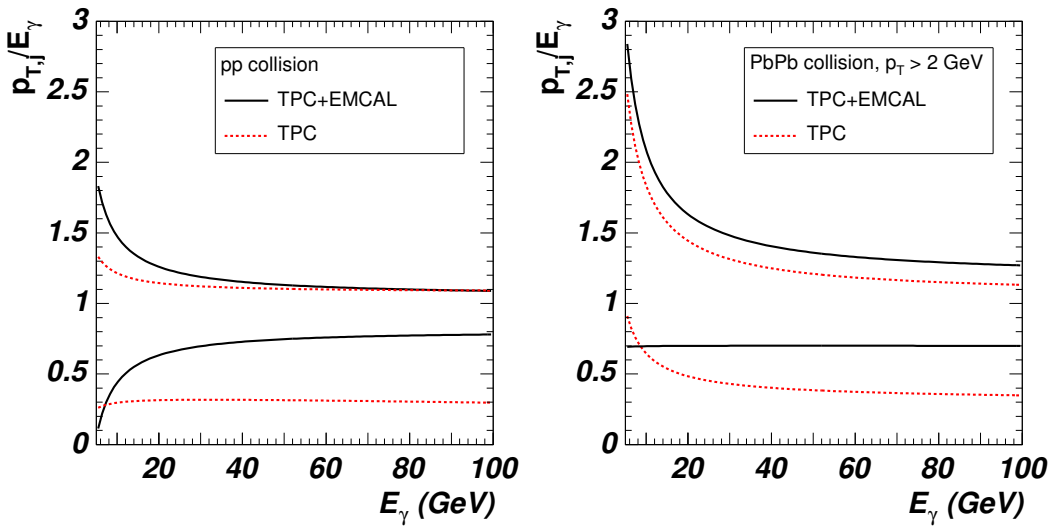

Figure 31: Maximum (upper line) and minimum values (lower line) to the ratio $p_{T,j}/E_\gamma$ to select a photon-jet event in the configuration with EMCal (solid line) and without EMCal (dashed line) in pp (left figure) and Pb-Pb collisions (right figure).

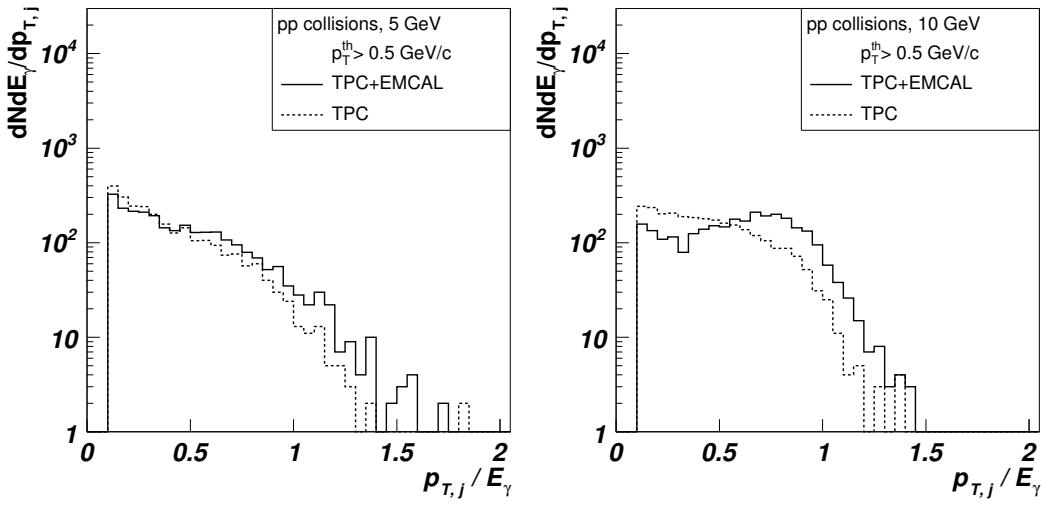

Figure 32: Simulated jet distribution as a function of the ratio $p_{T,j}/E_\gamma$ for low energy jets, 5 GeV (left) and 10 GeV(right), in pp collisions. A jet cone with $R = 0.3$ has been considered in all cases. There is a jet particle threshold of $p_T > 0.5$ GeV/c. In each subfigure the results for two experimental configurations are given: without EMCal (dashed line) and with EMCal (solid line).

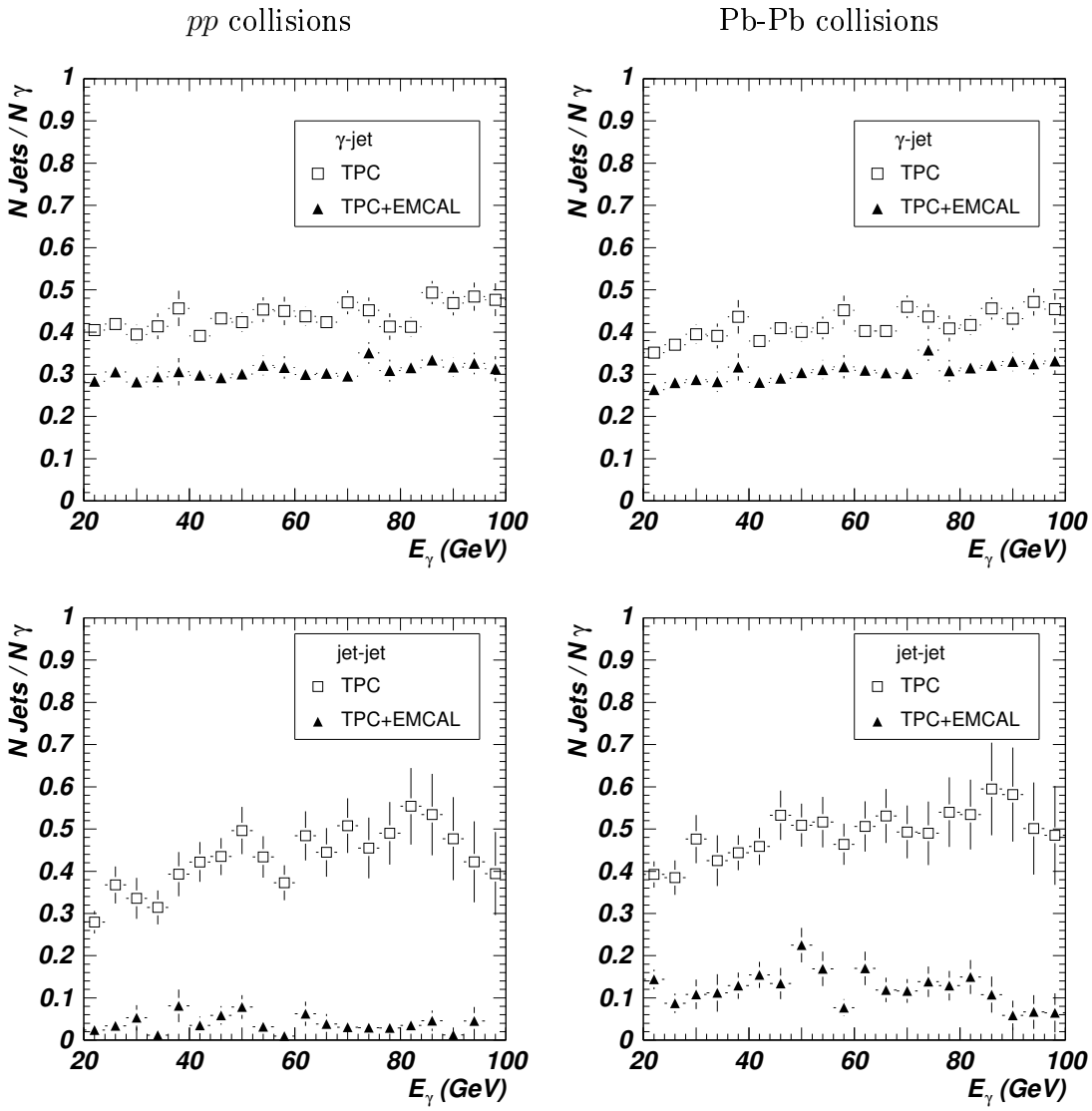

Figure 33: Upper frames: Jet selection efficiency, i.e., the number of accepted jets divided by the number of prompt photons detected in PHOS. Lower frames: Number of accepted jets (jet-jet events) divided by the number of γ-like particles (single and overlapped photons in jet-jet events) entering in PHOS. Figures shown for *pp* (left) and Pb-Pb (right) collisions. Two configurations have been studied, the TPC alone configuration (□), and the configuration TPC+EMCal (▲).

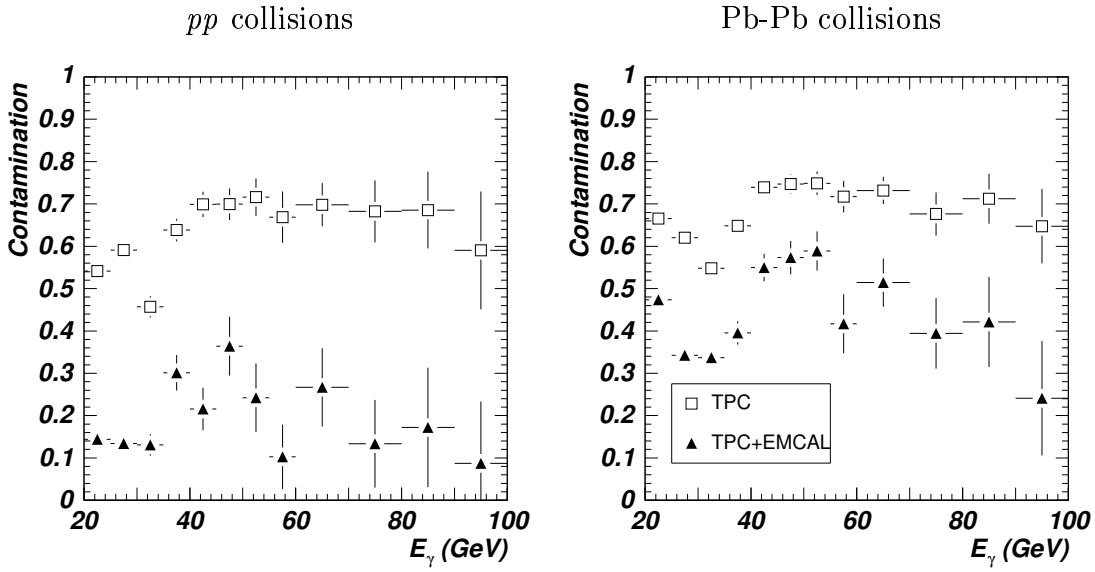

Figure 34: γ-tagging contamination. Left (right) frame correspond to pp (Pb-Pb) collisions. In this case there is no prompt photon identification in PHOS, just high p_T neutral signals trigger the jet algorithm.

purity of about 80 % and 60 % in the case of pp and Pb-Pb collisions (Fig. 34). For the TPC only configuration (Fig. 34), the achieved purity is worse and equal to about 20-40 %.

Switching on in PHOS a prompt photon trigger (PID and Isolation Cut identification), the obtained purities are greatly enhanced (Figs. 35). In pp collisions the purity reaches more than 80 % for the TPC alone configuration and plateaus at 100 % for the more complete TPC+EMCal configuration. As expected in Pb-Pb collisions, for the TPC+EMCal configuration, the purity decreases to 90 % at low E_γ but at 40 GeV it recovers almost to 100 % and the TPC alone configuration manifests the same behavior going from 80 % to about 90 %.

4.5 γ-jet correlations

To study quantitatively the interaction of jets with the medium, an adequate method is to study how the fragmenting hadrons are redistributed in phase space [8], i.e. by measuring the jet Fragmentation Function (FF). The experimental FF is the distribution of charged hadrons within a jet as a function of the variable z, defined for hard processes with a γ-jet in the final state as $z = \frac{p_T}{E_\gamma}$. FF's, as they would be measured in a standard year of running at LHC, have been calculated for γ-jet events in pp and Pb-Pb collisions, after proper identification as described in the previous section (Fig. 36). The FF's obtained for jet-jet events and misidentified as γ-jet events have been calculated too (Fig. 36). The distributions are obtained by integrating all events with parton energy larger than 20 GeV/c.

- For pp collisions, without considering any photon identification, neither PID nor ICMS, the contamination of misidentified jet-jet events dominates the real

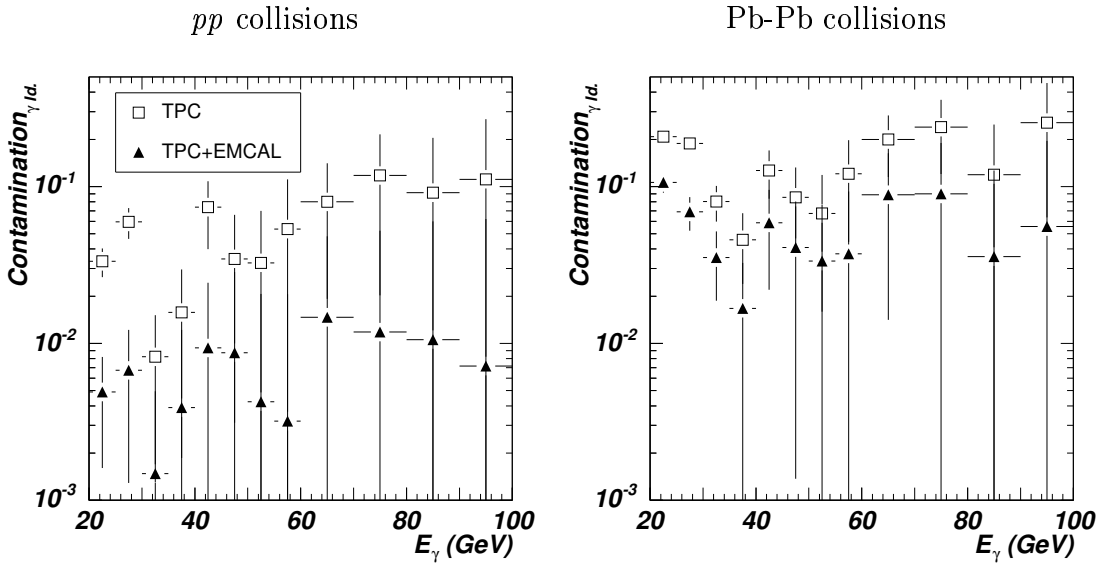

Figure 35: γ-tagging contamination. Left (right) frame correspond to pp (Pb-Pb) collisions. In this case there is no prompt photon identification in PHOS, just high p_T neutral signals trigger the jet algorithm. In this case prompt photon identification (SSA-PID + ICM) has been applied in PHOS.

γ-jet events in the absence of EMCal. Adding EMCal the contamination is suppressed leading to a signal to background value of about 4. Applying the two prompt photon identification methods (SSA-PID and ICMS), the contamination of misidentified jet-jet events is dramatically reduced leading to signal to background ratio of about 20 in the case of TPC only and close to 100 % background rejection with EMCal. At the same time the counting statistics of γ-jet events is reduced by about 10 % for medium purity photons (see Fig. 7-left), the ICMS does not reduce the statistics.

- For Pb-Pb collisions, the FF shows a strong rise at low z which is due to the low p_T hadrons from the underlying events. This contribution can be subtracted by calculating a pseudo-FF outside the cone of the leading particle. We constructed this pseudo-FF with the particles inside a cone of size $R = 0.3$, centered at $(\phi_{leading} - \pi,\ \eta_{leading})$. As in the case of pp collisions, the photon identification (SSA-PID and ICM) is required to suppress to an acceptable level the contamination of wrongly identified jet-jet events. The final signal to background ratio obtained is about 4 in the case of TPC only and rises to about 10 when adding EMCal. After the prompt photon identification the counting statistics of γ-jet events is reduced by about 60 % due to SSA-PID for medium purity photons ($\sim$25 %, see Fig. 7-right), and due to ICM ($\sim$50 %, see Tab. 4).

The FF's as they would be measured, i.e. the sum of properly identified γ-jet and wrongly identified jet-jet events, properly scaled are shown in Fig. 37. The statistical errors are calculated from the counting statistics in one standard year

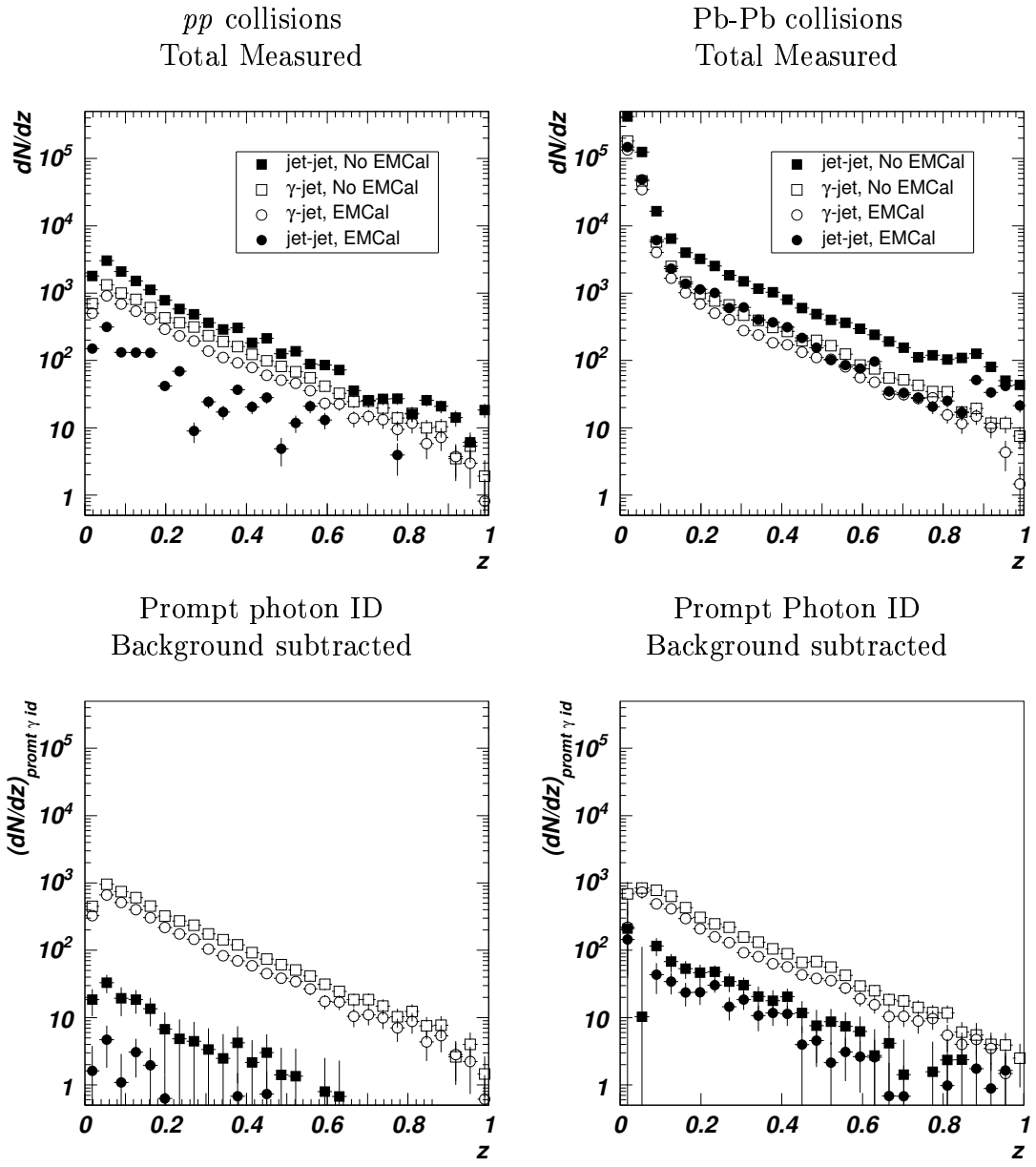

Figure 36: Fragmentation function for γ-jet and jet-jet events with energy larger than 20 GeV in *pp* (left) and Pb-Pb (right) collisions. The upper figures show the FF without prompt photon identification in PHOS and the lower figures show the FF if the prompt γ is identified in PHOS, and the background is subtracted.

of LHC running. The systematic errors reflect the amount of contamination. We have also considered the case where jet-jet events are quenched by the factor 5 as observed at RHIC. Without quenching, the systematic errors are similar than the statistical errors over the range $0.1 < z < 0.5$, whether EMCal is present or not. With EMCal the systematic errors become smaller, however the counting statistics is reduced by a factor of about 1.5 when comparing with the configuration without EMCal (Figs. 33), mainly because of the limited EMCal acceptance. When we consider quenching, the systematic errors are always smaller than the statistical ones, in both configurations.

To evaluate the sensitivity of the FF for photon-tagged jets to medium induced modifications, we have constructed the nuclear modification factor defined as the ratio of the FF measured in AA to the FF measured in pp scaled to the binary NN collisions, R_{FF}. This ratio is equal to 1 in absence of nuclear effects. We indeed recover a constant value equal to 1 over the entire z range (Fig. 38). Within this first approximation analysis, the statistical and systematical errors indicate that in the range $0.1 < z < 0.5$ (for greater and lower values the statistical fluctuations are large) we could be sensitive to a modification factor of the order of 5 % in both configurations. If we include a quenching factor of 5 to hadrons in jet-jet events and Pb-Pb collisions, this analysis indicates that we could observe variations of the order of the percent in both configurations, being only limited by the statistics.

Conclusion

We developed an algorithm to identify in ALICE prompt photons and γ-jet events generated in pp and Pb-Pb collisions at LHC energies. Prompt photons are identified efficiently in PHOS with the help of a shower shape analysis, capable to reject hadrons, and an isolation cut efficient to reject π^0 mesons. We estimated the spectrum of the identified prompt photons with the statistics of ALICE integrated luminosity in a standard year of running at LHC. The γ-jet events are identified by selecting a prompt photon in PHOS and searching for a leading particle in back to back correlation inside the ALICE central tracking system with or without an electromagnetic calorimeter. Jets are reconstructed by a cone algorithm with the found leading particle as seed and correlated with the photon through various conditions. The efficiency for identifying γ-jet events is limited mainly by the acceptance of the central tracking system and EMCal, to about 40 to 50 % if we use only the TPC and to about 30% if we combine them due to the smaller EMCal acceptance, for jets with energies larger than 20 GeV/c. Jet-jet cross sections are larger than γ-jet events and consequently they induce a considerable background resulting from photons originating from π^o decays detected in PHOS and misidentified as direct photons. With configuration including EMCal, these events are effectively rejected and reduced, to a negligible level of contamination, by applying shower shape and isolation cut analyses. Fragmentation functions can be accurately reconstructed and used to define a corresponding nuclear modification factor, R_{FF}. Will the sensitivity be sufficient to identify medium induced effects? This question will be answered in a forthcoming note where the effect of a elaborate jet quenching formalism will

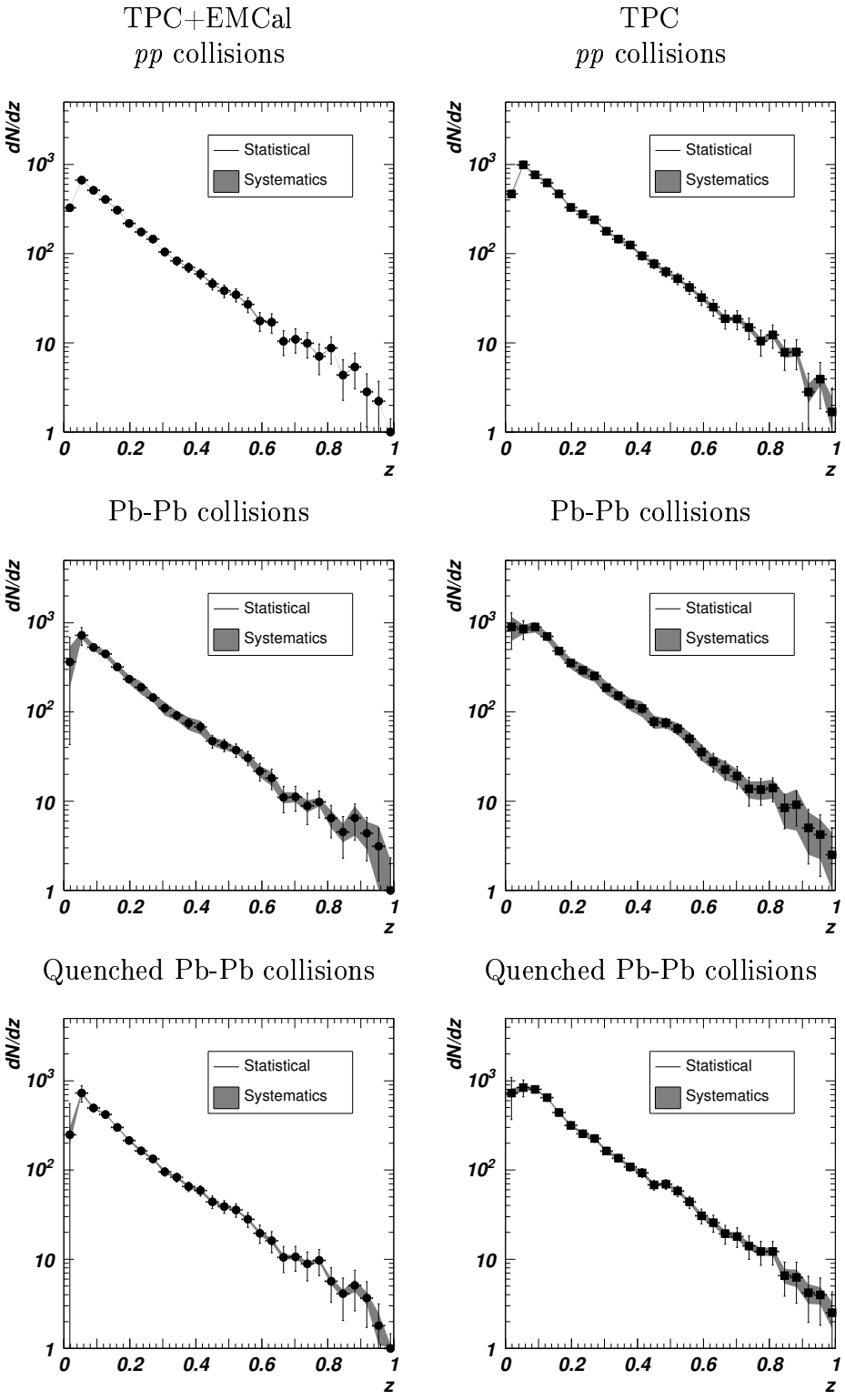

Figure 37: Fragmentation function of γ-tagged (γ-jet+jet-jet events after prompt photon identification) with energy larger than 20 GeV for a whole ALICE year, detected in the central tracking system or EMCal (left frames) or in the central tracking system only (right frames), in *pp* (upper frames), Pb-Pb (central row frames) collisions, and also considering a particle suppression factor of 5 in quenched Pb-Pb collisions (lower frames). The band shows systematic error due to the contamination of jet-jet events. Prompt photons detected in PHOS (medium purity photons)

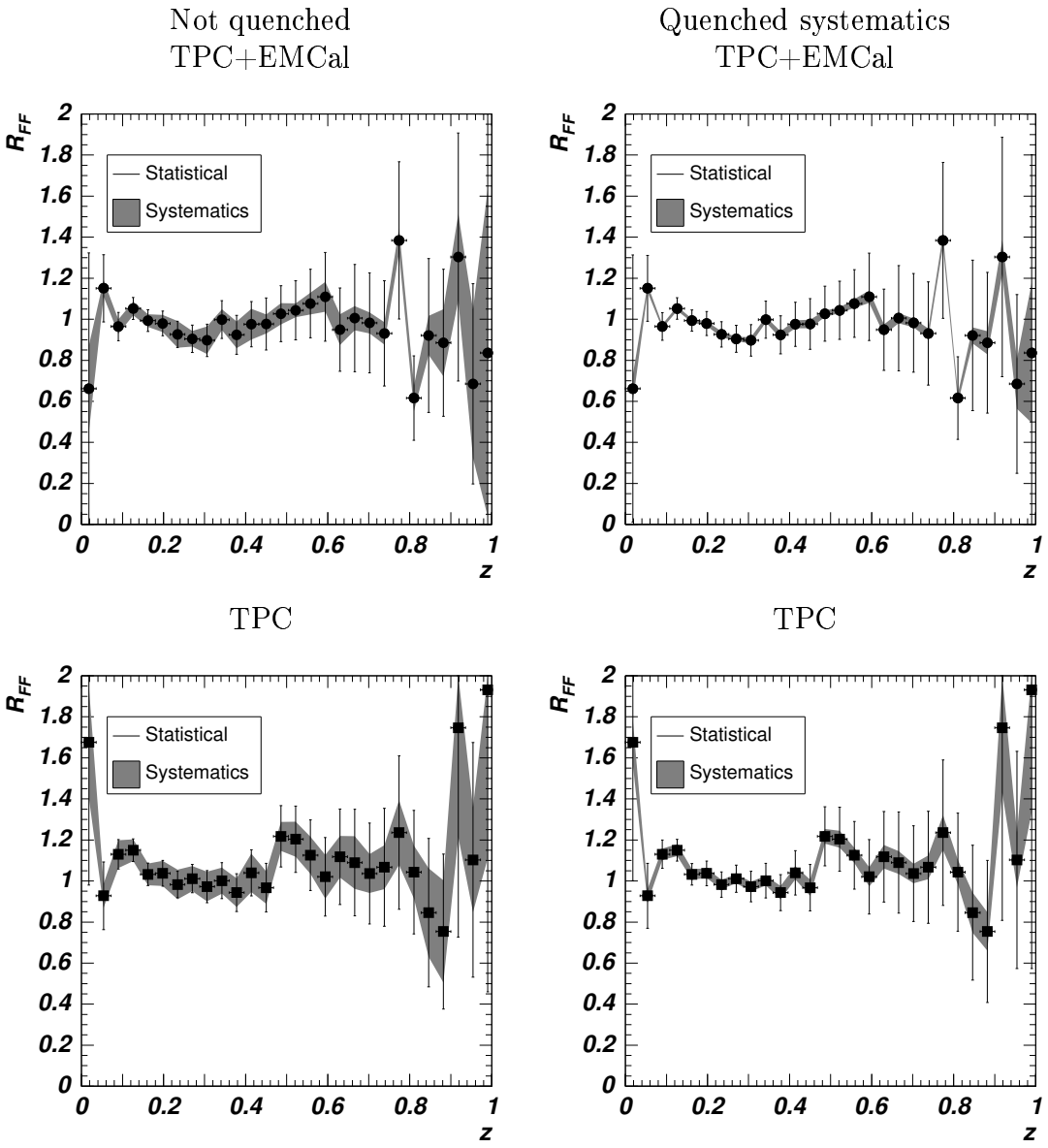

Figure 38: Ratio of the fragmentation functions of γ-tagged jets, γ-jet events, with energy larger than 20 GeV for Pb-Pb collisions scaled by Eq. (3) to *pp* collisions, detected in the central tracking system or EMCal (upper) or in the central tracking system only (lower). The band shows systematic error due to the contamination from jet-jet events. In left figures there is no quenching and in right ones the background in Pb-Pb collisions is quenched.

Table 10: Cross section and number of generated events for γ-jet events generated with PYTHIA *pp* collisions at $\sqrt{s_{NN}} = 5.5$ TeV, $|\eta_\gamma| < 0.2$ and $200^\circ < \phi_\gamma < 340^\circ$.

$< p_T >$(GeV/c)	σ (mb)	N events
20-40	1.16 10^{-6}	17,000
40-60	1.14 10^{-7}	14,500
60-80	2.53 10^{-8}	12,000
80-100	8.31 10^{-9}	9,500

Table 11: Cross section and number of generated events for jet-jet events generated with PYTHIA *pp* collisions at $\sqrt{s_{NN}} = 5.5$ TeV, with $|y_{parton}| < 0.2$, $|\eta_{jet}| < 0.15$.

$< p_T >$(GeV/c)	σ(mb)	N events
30-40	2.13 10^{-4}	178,500
40-50	6.68 10^{-5}	161,500
50-60	2.62 10^{-5}	141,000
60-70	1.19 10^{-5}	145,500
70-80	5.98 10^{-6}	151,500
80-90	3.29 10^{-6}	171,500
90-100	1.89 10^{-6}	154,000
100-150	2.97 10^{-6}	152,500
150-200	4.76 10^{-7}	86,500
200-250	1.20 10^{-7}	93,000
250-300	3.75 10^{-8}	136,000

be investigated. This work was supported by the FPI grant FP2000-5452 from the Spanish Ministry of Education and Science, the INTAS contract number 03-52-5747 and the EU contract HPMT-CT-2001-00346 from the "Marie Curie, Training Site" program.

A Cross sections

We generated PYTHIA γ-jet and jet-jet events of *pp* collisions at $\sqrt{s_{NN}} = 5.5$ TeV, with different p_T ranges. PYTHIA calculates the cross sections for these processes and the different momentum bins generated, and these values are shown in Tabs. 10 and 11. These events were generated for a restricted acceptance: for γ-jet events, the prompt photon pseudorapidity range is $\eta_\gamma < 0.2$ and the azimuth range is $200^\circ < \phi_\gamma < 340^\circ$; for jet-jet events, rapidity range in the subprocess center-of-mass system $|y_{parton}| < 0.2$ and pseudorapidity range of the final jets $\eta_{jet} < 0.15$.

References

[1] A. Accardi et al., *Hard probes in heavy ion collisions at the LHC: Jet physics* (2003), hep-ph/0310274.

[2] J. D. Bjorken, *Energy loss of energetic partons in quark - gluon plasma: Possible extinction of high p(T) jets in hadron - hadron collisions* (1982), FERMILAB-PUB-82-059-THY.

[3] K. Adcox et al. (PHENIX). *Suppression of hadrons with large transverse momentum in central Au + Au collisions at s**(1/2)(N N) = 130 GeV.* Phys. Rev. Lett. **88**, 022301 (2002), nucl-ex/0109003.

[4] K. Adcox et al. (PHENIX). *Centrality dependence of the high p(T) charged hadron suppression in au + au collisions at s(NN)**(1/2) = 130 GeV.* Phys. Lett. **B561**, 82 (2003), nucl-ex/0207009.

[5] C. Adler et al. (STAR). *Centrality dependence of high p(T) hadron suppression in Au + Au collisions at s(NN)**(1/2) = 130 GeV.* Phys. Rev. Lett. **89**, 202301 (2002), nucl-ex/0206011.

[6] S. S. Adler et al. (PHENIX). *Suppressed pi0 production at large transverse momentum in central Au + Au collisions at s(NN)**(1/2) = 200 GeV.* Phys. Rev. Lett. **91**, 072301 (2003), nucl-ex/0304022.

[7] C. A. et all (STAR collaboration). *Disappearance of back-to-back high p_T hadron correlations in central Au+Au collisions at $\sqrt{s_{NN}}$ = 200 GeV.* Phys. Rev. Lett. **90**, 082302 (2003).

[8] C. A. Salgado and U. A. Wiedemann. *Medium modification of jet shapes and jet multiplicities.* Phys. Rev. Lett. **93**, 042301 (2004), hep-ph/0310079.

[9] F. Arleo, P. Aurenche, Z. Belghobsi, and J.-P. Guillet. *Photon tagged correlations in heavy ion collisions.* JHEP **11**, 009 (2004), hep-ph/0410088.

[10] PHOS Collaboration, *Photon identification in ALICE performance* (2005), chap. 5 of ALICE Physics Performance Report.

[11] T. M. Cormier. *Jet physics in alice with a proposed electromagnetic calorimeter.* Eur. Phys. J. **C34**, s333 (2004).

[12] T. Sjostrand et al. *High-energy physics event generation with PYTHIA 6.1.* Comput. Phys. Commun. **135**, 238 (2001a), hep-ph/0010017.

[13] T. Sjostrand, L. Lonnblad, and S. Mrenna. *PYTHIA 6.2: Physics and manual.* hep-ph/0108264 (2001b).

[14] M. Gluck, E. Reya, and A. Vogt. *Dynamical parton distributions of the proton and small x physics.* Z. Phys. **C67**, 433 (1995).

[15] M. Gyulassy and X.-N. Wang. *HIJING 1.0: A monte carlo program for parton and particle production in high-energy hadronic and nuclear collisions.* Comput. Phys. Commun. **83**, 307 (1994), `nucl-th/9502021`.

[16] F. Arleo et al., *Photon physics in heavy ion collisions at the LHC* (2003), `hep-ph/0311131`.

[17] H. Delagrange (ALICE), *Predictions for high p_T and π^0 production at ALICE/LHC*, ALICE-INT-2002-02-v 1.0 (2002).

[18] *Alice offline project* (2000), URL `http://aliceinfo.cern.ch/Offline/`.

[19] ALICE Collaboration. *Technical design report ITS.* ALICE TDR **4** (1999).

[20] ALICE Collaboration. *Technical design report TPC.* ALICE TDR **7** (2000).

[21] M. Kowalski (ALICE), *Presentation at the TPC meeting (29-30/04/2002)* (2002), ALICE-PR-2002-131.

[22] K. Adcox et al. (PHENIX). *Formation of dense partonic matter in relativistic nucleus nucleus collisions at RHIC: Experimental evaluation by the PHENIX collaboration.* Nucl. Phys. A **757**, 184 (2005), `nucl-ex/0410003`.